Consecutive charging and discharging of a PCM-based plate heat exchanger with zigzag configuration

Pouyan Talebizadeh Sardari [a], Jasim M. Mahdi [b], Hayder I. Mohammed [c], M.A. Moghimi [d], Amir Hossein Eisapour [e], Mohammad Ghalambaz [f, g, *]

[a] Centre for Sustainable Energy Use in Food Chains, Institute of Energy Futures, Brunel University London, Kingston Lane, Uxbridge, Middlesex, UB8 3PH, UK
[b] Department of Energy Engineering, University of Baghdad, Baghdad 10071, Iraq
[c] Department of Physics, College of Education, University of Garmian, Kurdistan, Iraq
[d] Department of Engineering and Design, Staffordshire University, Stoke-On-Trent ST4 2DE, UK
[e] Department of Energy and Aerospace Engineering, School of Mechanical Engineering, Shiraz University, Shiraz, Iran
[f] Metamaterials for Mechanical, Biomechanical and Multiphysical Applications Research Group, Ton Duc Thang University, Ho Chi Minh City, Viet Nam
[g] Faculty of Applied Sciences, Ton Duc Thang University, Ho Chi Minh City, Viet Nam

ARTICLE INFO

ABSTRACT

Due to the remarkable energy savings, isothermal nature of the operation and low costs, energy storage with phase-change materials (PCMs) is a reliable technology for filling the gap between energy supply and demand. In this paper, an attempt has been made to modify the storage functionality of PCM in a plate type heat exchanger with zigzag configuration. A two-dimensional, time-dependent simulation model for the PCM phase transition during the charging and discharging modes has been developed and validated via earlier related findings. The effects of zigzag angle orientation, inlet flowrate and mean temperature of the heat transfer fluid (HTF) are thoroughly studied and revealed. Results show that increasing the angle of zigzag orientation has no noticeable impact on the development of phase transition during the early stages of operation. However, this effect becomes more noticeable and almost leads to faster storage/retrieval rates as time further elapses. It is found that the system with the zigzag angle of 60° augments the storage rate by 32.6% compared with the system of 30° zigzag angle. Also, higher HTF temperature and/or higher Reynold number result in faster phase-transition rates during both parts of the energy charging-discharging cycle.

Nomenclature

A_m	Mushy zone constant
C_p (Jkg^{-1}K^{-1})	Specific heat
g (ms^{-2})	Gravity
k (Wm^{-1}K^{-1})	Thermal conductivity
L_f (Jkg^{-1})	Latent heat of fusion
m (kg)	Mass
P (Pa)	Pressure
Q (J)	Thermal storage/recovery capacity
$\dot{Q}$ (W)	Thermal storage/recovery rate
T_L (°C)	Liquidus temperature
T_S (°C)	Solidus temperature
$\vec{V}$ (m/s)	Velocity
t_m (s)	Melting/solidification time
T (°C)	Temperature
T_e (°C)	End temperature
T_i (°C)	Initial temperature

Greek symbols

α (degrees)	mid-wall zigzag angle
β (K^{-1})	Expansion coefficient
λ	Liquid fraction
μ (kgm^{-1}s^{-1})	Dynamic Viscosity
ρ (kgm^{-3})	Density
ΔH (Jkg^{-1})	Latent heat of fusion

* Corresponding authors at: Ton Duc Thang University, Ho Chi Minh City, Viet Nam.
E-mail addresses: pouyan.talebizadehsardari@brunel.ac.uk (P. Talebizadeh Sardari), mohammad.ghalambaz@tdtu.edu.vn (M.Ghalambaz).
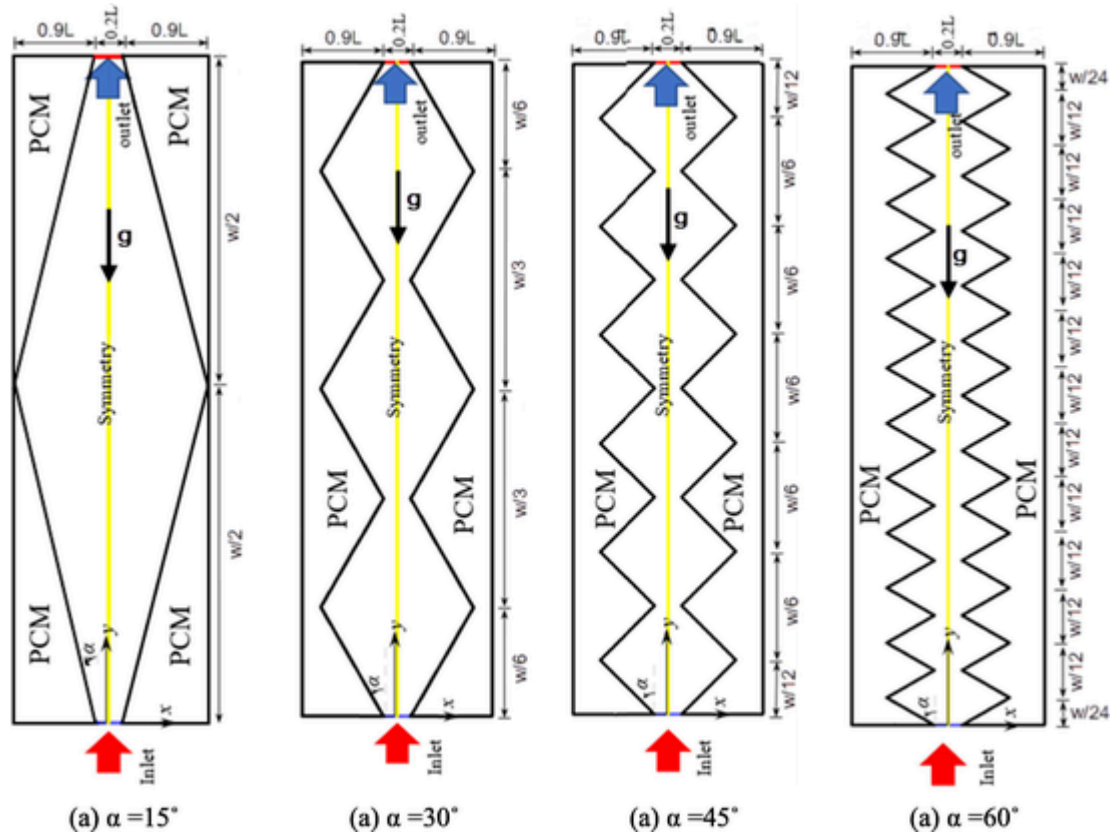
Fig. 1. Schematic diagram (not-to-scale) showing the studied heat exchanger with a zigzag plate configuration.

Table 1
Thermo-physical properties of RT35 [40].

Property	ρ_l [kg/m³]	ρ_s [kg/m³]	L_f [kJ/kg]	C_p [kJ/kg.K]	k [W/m.K]	μ [N.s/m²]	T_L [°C]	T_S [°C]	β [1/K]
values	770	860	170	2.0	0.2	0.023	36	29	0.0006

1. Introduction

The tendency to depend on fossil fuels to meet the energy demand is continuously growing worldwide, and the future scarcity of fossil fuel sources is predicted [1]. The share of fossil fuel is still about 75% of the total global energy consumption [2]. The use of fossil fuels is responsible for environmental problems such as climate change and atmospheric pollution, which have a direct impact on the quality of human life. Thus, efforts to develop more efficient technologies to harness the energy from clean and renewable sources like sunlight and wind are required. Solar energy is ranked as the most promising free source of energy and is directly connected to utilizing efficient energy storage systems to address its intermittent supply nature. In this regards, Thermal energy storage (TES) would act as a connector between the energy supply and use, enhancer of the system efficiency and favourable saver of energy [3,4]. TES systems can be categorized into three main groups: sensible heat TES, latent heat TES and thermochemical TES. The key function of TES components is to eliminate energy wastages and their major costs to allow fabrication of more cost-effective energy conversion systems. Phase change materials (PCMs) based application is considered among the most promising technologies to store and retrieve thermal energy demand [5]. It is necessary to understand and cover all issues and contradictions related to this technology before moving to the next step of application in the large-scale theme.

Usually, PCMs are poor in thermal conductivity and require heat transfer augmentation such as using multiple PCMs, embedding solid porous matrices, employing fins and utilizing a zigzag surface exten-

sion. The method of multiple PCM performed by many researchers [6–12]. Gong and Mujumdar [8] modelled an innovative multiple PCM storage system consisting of coaxial cylinder internally holding layers of different PCMs. Their outcome showed that using the multiple PCM has a great influence on the melting and solidification phases by reducing the outlet temperature of the HTF. Around 34% faster heat transfer rate was reported when layers of multiple PCMs were used. The effects of multiple PCMs on the efficiency of different TES systems were numerically evaluated by Fang and Chen [7]. They stated that the different phase transition temperature between the PCM layers is very vital for efficiency improvement of the system. Seeniraj and Narasimhan [10] stated that multiple PCM provides almost the same flow exit temperature for a very long duration. Kurnia et al. [13] developed a novel festoon configuration using multiple PCMs in four different ways. They reported much better heat transfer rate in the festoon design compared to the corresponding U-tube shape. The predictions of heat transfer rate showed more improvement with the use of multiple PCMs. Previous research generally shows that utilizing multiple PCMs improves the heat transfer rate, thus saving the time of the melting-solidification process. The natural convection flow in a molten region is another important effect that contributes to a better heat transfer rate and significantly reduces the melting solidification time. Thus, natural convection has an important role to play during melting of PCMs in the large and medium-size enclosures. It also should be considered when computation on problems involving melting is performed. Various aspects of the heat transfer associated with PCM melting involving natural convection flows has been investigated in several recent studies [14–18].
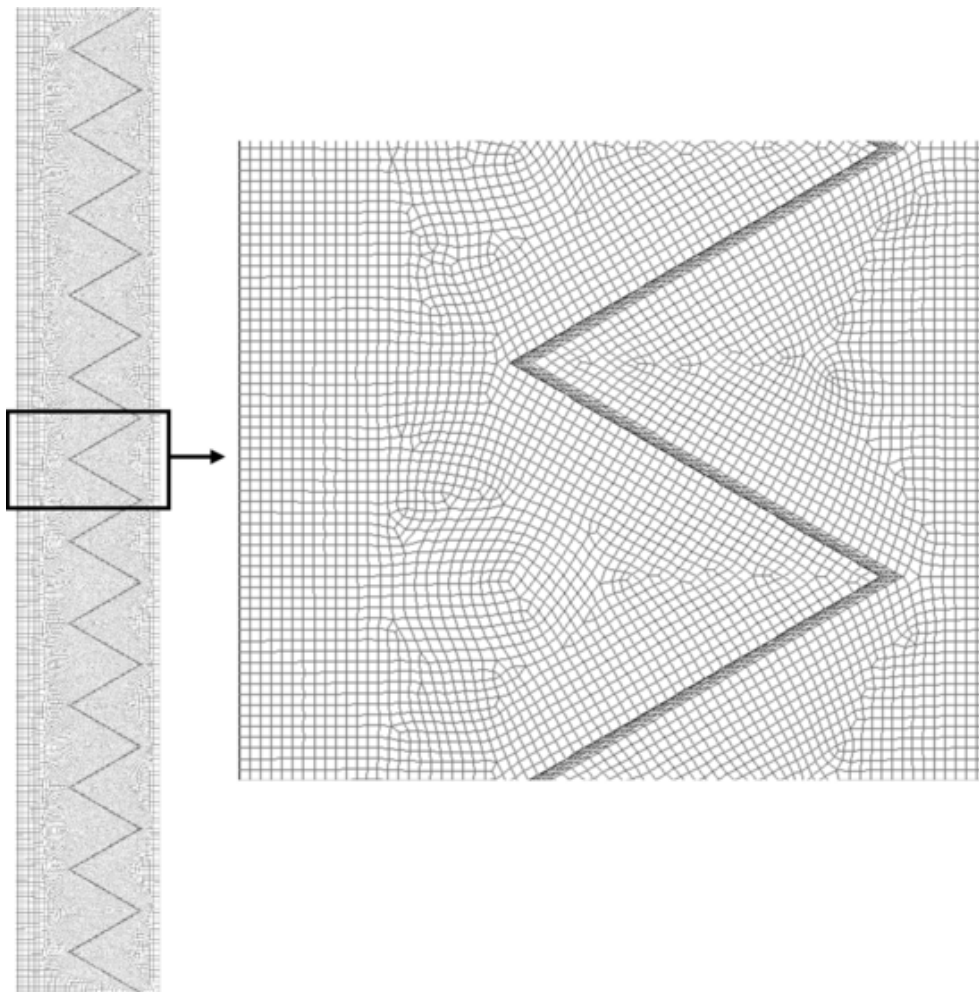
Fig. 2. The mesh of the longitudinal section of the system covering the PCM and the fluid flow areas.
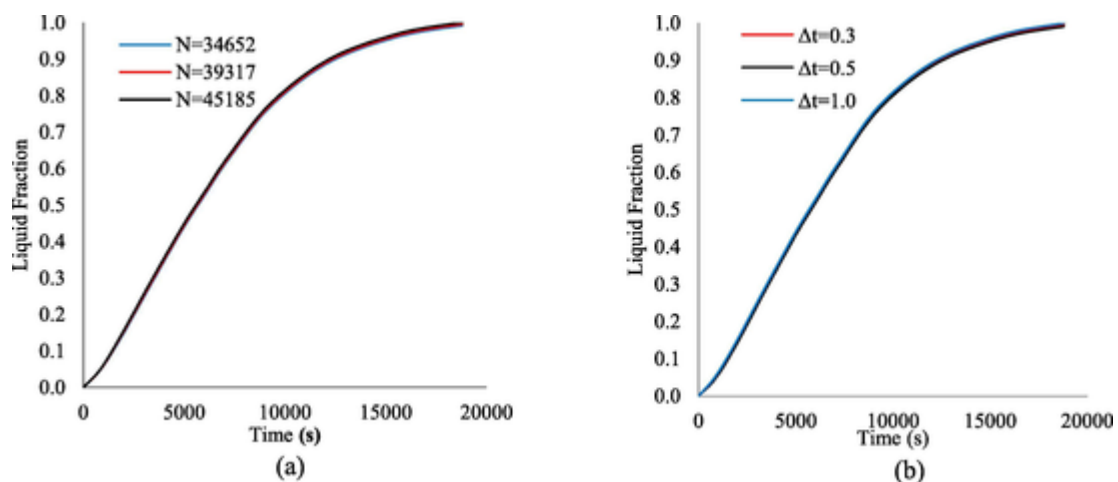

Fig. 3. The numerical solution independency tests for (a) the mesh size and (b) the time step.

Adding fins (longitudinal, radial) to augment the heat transfer rate in the latent heat TES systems while increasing the heat-exchange surface area is very widespread. Many studies cover the application of longitudinal fins to enhance the melting-solidification processes [19–30]. Shokouhmand and Kamkari [31] studied the melting process of the PCM using longitudinal fins on the horizontal tube. They found that the PCM melting rate is proportional to the number of fins because of expanding the heat transfer area in use. Rathod and Banerjee [22] experi-

mentally studied the charging-discharging processes of the TES under the effect of three longitudinal fins. They found that the rate of energy storage mode and recovery could be improved by 24.52% and 43.6%, respectively. Radial fins also studied by many researchers [32–34]. Choi and Kim [35] used circular fins in TES for solidification enhancement of (MgCl2·.6H2O) as a composite PCM. It was reported that circular fins could raise the heat transfer coefficient by 3.5 times over the plain tube. Also, they stated that the mass flow rate of heat-transfer
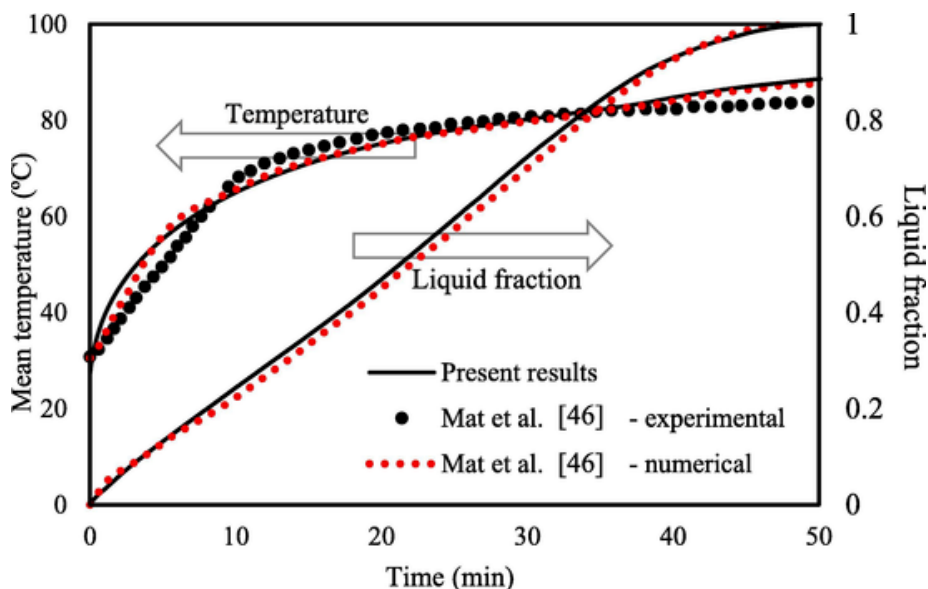
Fig. 4. Code verification comparing with the data of Mat et al. [46].

fluid (HTF) has a considerable influence on the heat transfer rate when fins are used compared to the non-finned system. Wang et al. [25] numerically evaluated the performance of LHSU, they suggested the use of fins with smaller pitch and higher fin radius because there was the insignificant effect when the fin pitch is being four times greater than their tube radius.

Applying zigzag configuration to extend the heat exchange surface also improves the thermal performance of latent TES systems. Wang et al. [36] explored the effect of applying multiple PCM and zigzag surface configuration on the melting of PCM in plate heat exchanger devise. As the author focused on the multiple-PCM, they found that using m-PCMs accelerated the melting rate in comparison with utilizing a single PCM. Also, there is a noticeable improvement in the melting rate recognised if a larger temperature difference exists between the m-PCMs. In another work, Wang et al. [11] studied the discharging process for the m-PCM with a zigzag surface topology in plate type heat exchanger. They stated that the zigzag surface topology with multiple PCMs can bring a very positive impact on the temperature uniformity and the overall discharge process.

This study aims to examine zigzag plate heat exchangers during melting and solidification processes. The PCM is placed in the outer shell while water is passed through the centre of the unit to exchange heat to/from the PCM. The inner and outer shells are separated by a zigzag plate. Different angles of the zigzag plate are investigated with different flow temperatures and Reynold numbers of the heat transfer fluid for which, to the best of the authors' knowledge, little has been done on the optimum pattern of the zigzag plate. No studies have been found in the literature on the influence of the mid-wall zigzag angle combined with effects of the HTF flow velocity and the average temperature on the overall energy charging-discharging process. Optimising the thermal performance would be a very important procedure to secure efficient thermal energy storage and recovery cycle for more practical applications of the latent heat TES systems.

2. Problem description

A latent-heat TES system with a vertical zigzag plate configuration is numerically investigated in this paper as shown in Fig. 1. Four different angles are studied for the zigzag configuration. Different angles of 15°, 30°, 45° and 60° are investigated as displayed in Fig. 1-a, 1-b. 1-c and 1-b, respectively. The angles are set in a way that the number of zigzags in different cases of 15°, 30°, 45° and 60° are 1, 3, 6 and 12, re-

spectively. The zigzag is created in a way that by starting from the beginning point, after one zigzag period, a point with the same distance from the centre is achieved. This pattern is repeated until reaching the end of the heat exchanger. The effects of inlet flow temperature and the Reynolds number of heat transfer fluid (HTF) are also examined where water is used as the HTF. The boundary conditions are also illustrated in Fig. 1 using constant velocity and temperature for the HTF inlet, outflow for the HTF outlet and adiabatic walls for the PCM domain. Due to the nature of the computational domain, only half of the proposed system are evaluated using symmetry boundary condition. The wall between the PCM and HTF is considered copper of 2-mm thickness. The flow of HTF between the zigzag plates is managed in compliance with the laminar regime conditions. Note that in Fig. 1, the total height of the heat exchanger is shown as *W* and the total the heat exchanger width is presented as *2L*.

Paraffin RT-35 is utilised as the PCM whose thermophysical properties are summarized in Table 1. Practically, there are several impacts could nullify the operation of the heat energy storage, such as the limited energy density, material compatibility, properties variation during the phase change process [37], corrosion, phase separation, lack of thermal stability and in inflammability [38]. The numerical work of this study assumed that there are no corrosions, the system is thermally stable, and the materials are not flammable. Because of the narrow differences between the properties of the liquid and solid phases of RT35, these properties considered to be constant. Moreover, during the numerical simulation in this study, the effect of natural convection is considered. However, volume expansion is neglected in this study since the focus of this study is on presenting an enhancement method to increase the phase change process. From the mechanical point of view in practical application, the required volume for the PCM expansion should be considered for example at the top of the PCM shell which is far from the heat transfer zone between the HTF and PCM in this study [39]. Also, due to considering insulation for the top wall of the PCM shell in this study to eliminate the environmental effects, the influence of considering an extra volume with no PCM is negligible on the results of the presented enhancement technique in this paper.
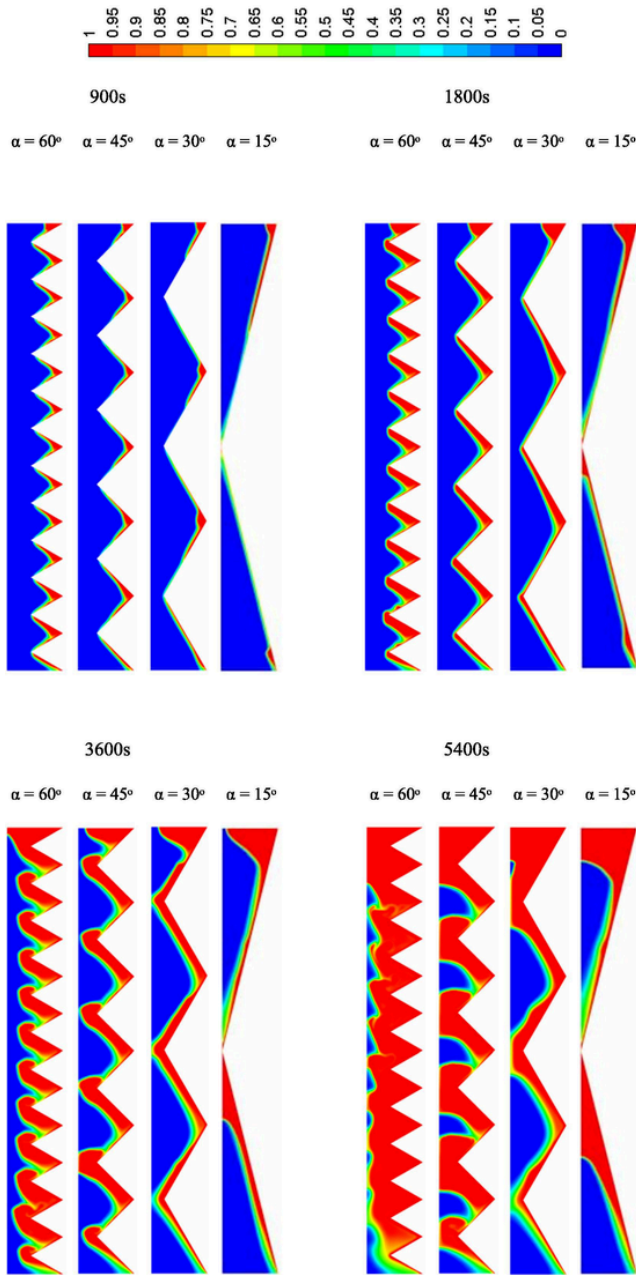
Fig. 5. Liquid-fraction contours at various time durations and various angles of zigzag configuration during the melting of PCM at T_{HTF} = 50 °C.

3. Mathematical modelling

3.1. Formulation of the governing equations

The enthalpy-porosity scheme [36,41–43] is implemented to formulate the equations which govern the conservation of mass, momentum, and energy for the three different zones involved, i.e. the HTF, the PCM and the copper wall between them as below:

Conservation of mass:

$$\frac{\partial \rho}{\partial t} + \nabla \cdot \rho \vec{V} = 0 \tag{1}$$

Conservation of x-momentum:

$$\frac{\partial (\rho u)}{\partial t} + \nabla \cdot \left(\rho u \vec{V} \right) = -\frac{\partial P}{\partial x} + \nabla \cdot (\mu \nabla u) - \frac{A_m (1-\beta)^2}{\lambda^3 + 0.001} u \tag{2}$$
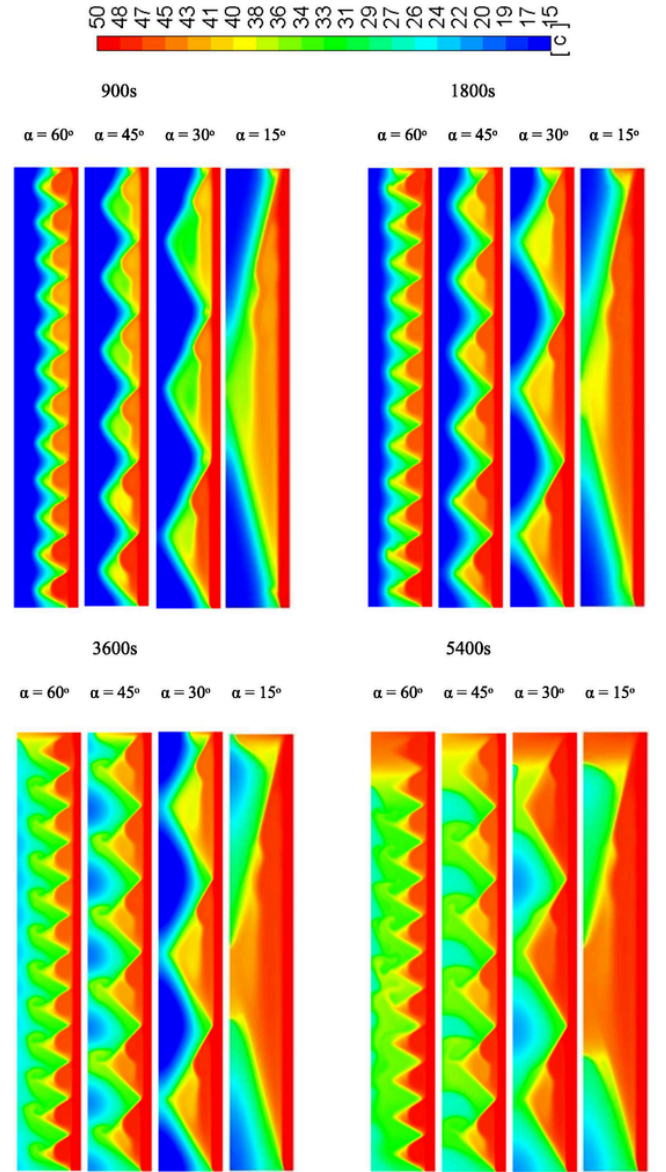

Fig. 6. Temperature contours (in °C) at various time durations and various angles of zigzag configuration during the melting of PCM at T_{HTF} = 50 °C.

Conservation of y-momentum:

$$\frac{\partial (\rho v)}{\partial t} + \nabla \cdot \left(\rho v \vec{V} \right) = -\frac{\partial P}{\partial y} + \nabla \cdot (\mu \nabla v) - \rho g \beta \left(T - T_{ref} \right) - \frac{A_m (1-\beta)^2}{\lambda^3 + 0.001} v \tag{3}$$

Conservation of energy:

$$\frac{\rho C_p \partial T}{\partial t} + \nabla \left(\rho C_p \vec{V} T \right) = \nabla \left(k \nabla T \right) - \left[\frac{\partial \rho \lambda L_f}{\partial t} + \nabla \left(\rho \vec{V} \lambda L_f \right) \right] \tag{4}$$

The following assumptions are employed for driving the governing equations as follows [44,45]:

- Boussinesq approximation for predicting the temperature-based density variation is valid.
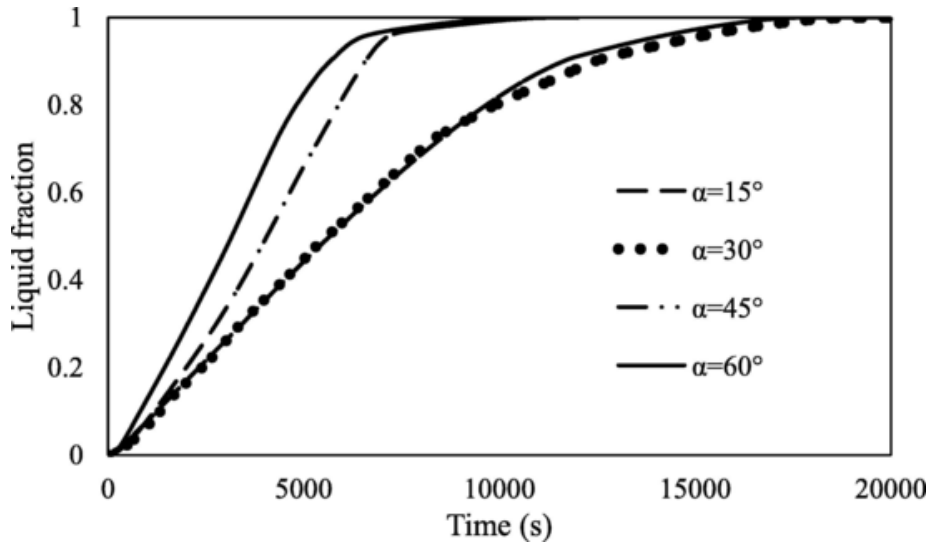- The flow of molten PCM is transient, Newtonian and laminar.

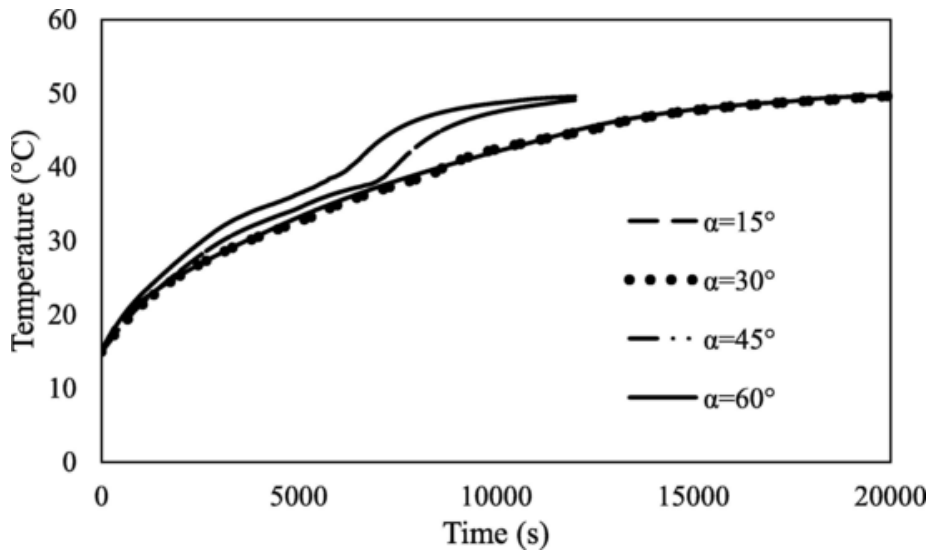Fig. 7. Transient variations of the PCM liquid fraction during melting at the zigzag angle of α = 15°, 30°, 45°, and 60° at T_{HTF} = 50 °C.

Fig. 8. Transient variations of the PCM average temperature during melting at the zigzag angle of α = 15°, 30°, 45° and 60° at T_{HTF} = 50 °C.

Table 2
Effect of applying different zigzag angles on the melting time, heat storage capacity and heat storage rate in the zigzag PCM channel.

α (°)	PCM mass (kg)	Melting time (s)	Heat storage capacity (J)	Heat storage rate (W)	ΔP (Pa)	Pumping power (W)
15	11.73	17,574	2,691,284	153.14	348.5	95.3
30	14.44	18,184	3,343,000	183.84	428.6	117.2
45	15.65	11,224	3,554,370	316.68	464.6	127.3
60	16.70	10,429	3,805,070	364.82	495.8	135.8

- Viscous dissipation is disregarded due to the lack of large enough, effective velocities.
- Heat loss to the surrounding is neglected due to the perfect insulation at the outer surface.
- No-slip boundary conditions are assumed at the inter walls
- The value 10^5 kg/m³s for A_m is selected based on the open literature [39,46–48]
- Volume expansion is neglected [49,50]

λ is introduced as [51]:

$$\lambda = \frac{\Delta H}{L_f} = \begin{cases} 0 \, if \, T < T_{Solidus} \\ 1 \, if \, T > T_{Liquidus} \\ \frac{T - T_{Solidus}}{T_{Liquidus} - T_{Solidus}} \, if \, T_{Solidus} < T < T_{Liquidus} \end{cases} \qquad (5)$$

A detailed description of the mathematical model can be found in the authors' previous work [41,44]. The total sum of sensitive enthalpy (h) and latent heat (ΔH) is the volumetric enthalpy (H):

$$H = h + \Delta H \qquad (6)$$

where

$$h = h_{ref} + \int_{T_{ref}}^{T} C_p dT \qquad (7)$$

and ΔH is calculated based on Eq. (4).

The thermal energy storage or recovery rate $\dot{Q}$ is defined as [52]:

Table 3
Effect of applying different HTF inlet temperature on the melting time and heat storage rate in the zigzag PCM channel.

| Inlet HTF temperature (°C)	Melting time (s)		Heat storage rate (W)	
	$\alpha = 30°$	$\alpha = 60°$	$\alpha = 30°$	$\alpha = 60°$
45	27,726	14,081	114.08	260.70
50	18,784	10,430	175.63	364.82
55	15,530	8685	221.12	455.16

$$\dot{Q} = \frac{Q}{t_m}$$

$$= \frac{m \left(\int_{solid} c_p dT + L_f + \int_{liquid} c_p dT \right)}{t_m} \tag{8}$$

$$\approx \frac{m(c_p \left(T_L - T_i \right) + L_f + c_p \left(T_e - T_S \right))}{t_m}$$

Note that for the water flow in the inner and outer tubes, the governing equations are the conventional Navier-Stokes equations which can be achieved by omitting the extra source terms from Eqs. (2)–(4). The rate of increase in pumping power consumption due to the increase in the circulation rate ($\dot{V}_{HTF}$) of the HTF through the TES unit is estimated as [43]:

$$PP = \left(\dot{V}_{HTF} \Delta P_{HTF} \right) \tag{9}$$
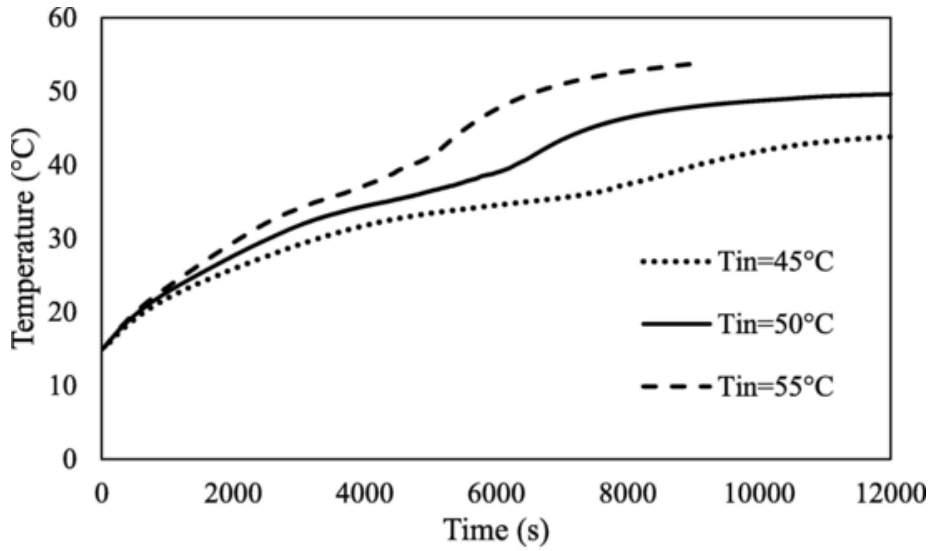

a) α=60⁰
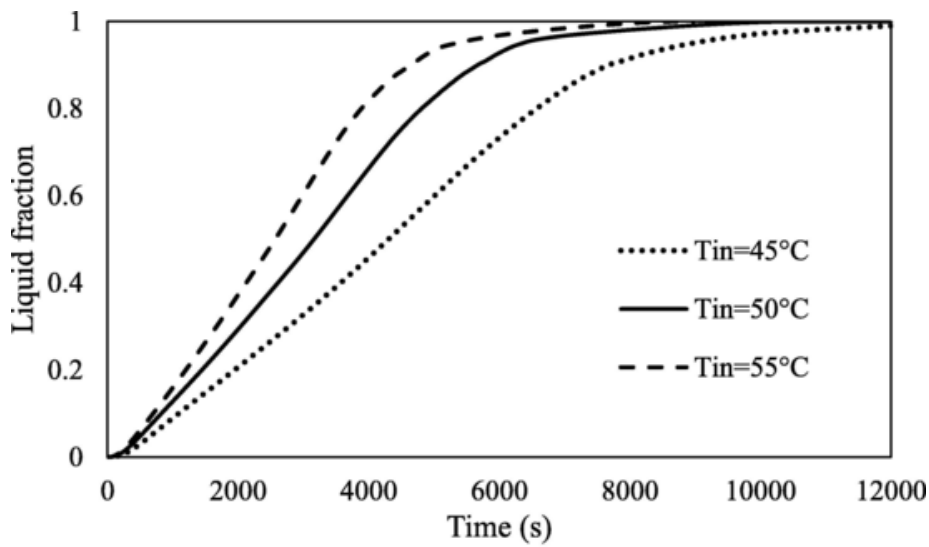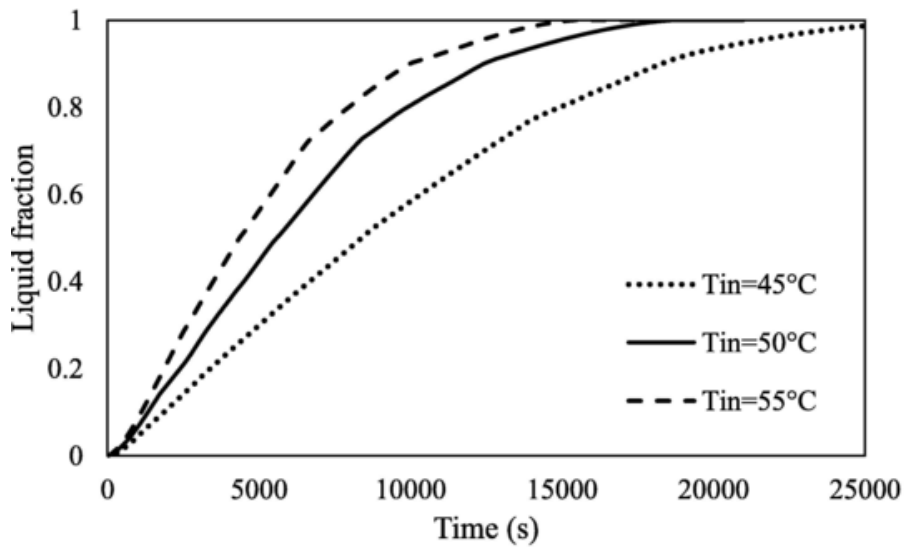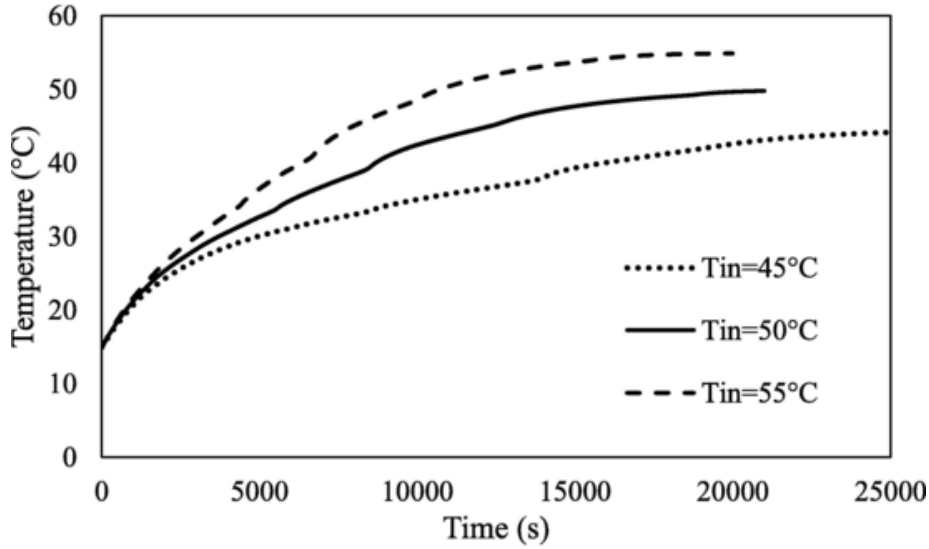

b) α=30⁰

Fig. 9. Transient variations of the PCM liquid fraction for the case with a) $\alpha = 60°$ and b) $\alpha = 30°$ during melting at $T_{in} = 45$, 50, and 55 °C.

a) α=60⁰

b) α=30⁰

Fig. 10. Transient variations of the PCM average temperature for the case with a) $\alpha = 60^0$ and b) $\alpha = 30^0$ during melting at $T_{HTF} = 45$, 50, and 55 °C.

3.2. Formulation of the initial and boundary conditions

The entire unit is initially assumed to be at 15 °C temperature for charging mode, which is adequate to guarantee that melting starts from fully solid PCM because the solidus temperature is 29 °C. For discharging mode, the initial unit temperature is fixed at 50 °C to ensure that solidification starts from fully liquid PCM as the liquidus temperature is 36 °C. The initial conditions are therefore formulated as:

$$At \ t = 0 \rightarrow \begin{cases} u = 0, v = 0, T = T_{int} = 15°C \ for \ melting \\ u = 0, v = 0, T = T_{int} = 50°C \ for \ solidifying \end{cases} \quad (10)$$

The boundary conditions for the inlet and outlet of the HTF channel can also be formulated as:

$$For \ inlet \rightarrow \begin{cases} u = 0, v = 0.0277 m/s, T_{inlet} = 50°C \ for \ melting \\ u = 0, v = 0.0554 m/s, T_{inlet} = 15°C \ for \ solidifying \end{cases} \quad (11)$$

For outlet → outflow boundary condition ($\dot{m}_{out} = \dot{m}_{in}$)

It should be noted that the velocity of HTF at the inlet is chosen to have the Reynolds number of 1000 based on the area of the inlet and properties of the water according to its temperature at the inlet. Therefore, due to the variation of the HTF viscosity and density during the melting and solidification, different values are employed for the HTF velocity at the inlet.

At the heat exchange interfaces between HTF and the zigzag plates or between zigzag plates and the PCM, continuous heat flow is assumed as follows:

$$T_{HTF}|_{\Omega_1} = T_{plate}|_{\Omega_1}$$
$$T_{plate}|_{\Omega_2} = T_{PCM}|_{\Omega_2} \quad (12)$$

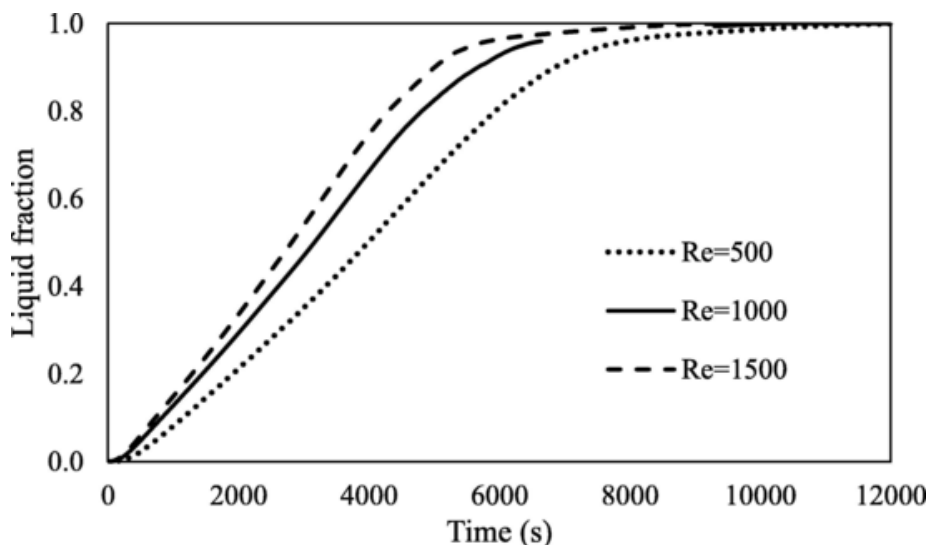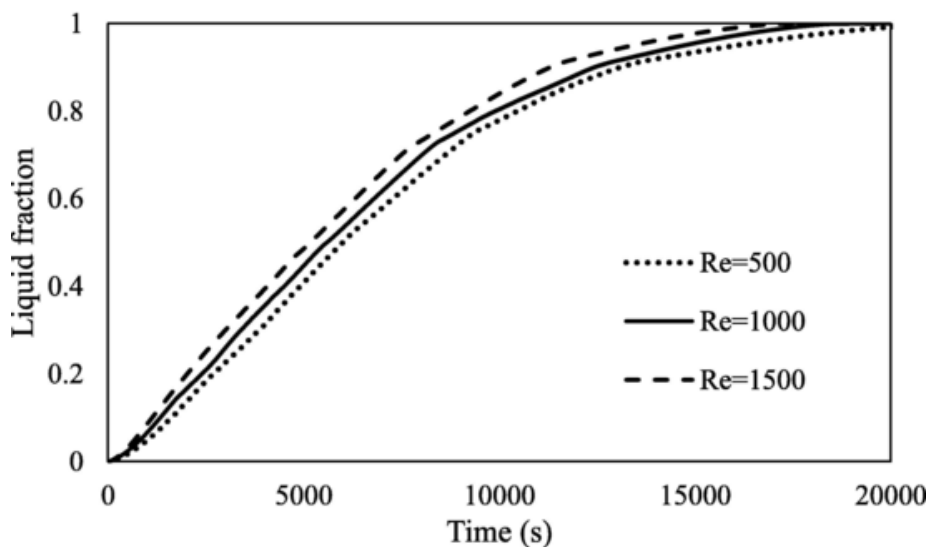where Ω_1 and Ω_2 refer to the heat exchange interfaces shared by HTF, zigzag plates, and PCM.
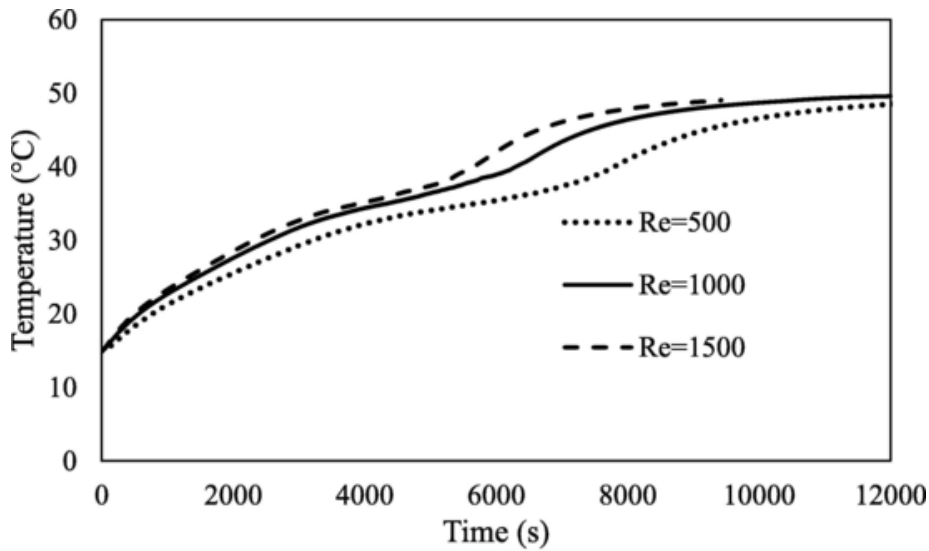
a) α=60⁰

b) α=30⁰

Fig. 11. Transient variations of the PCM liquid fraction for the case with a) $\alpha = 60^0$ and b) $\alpha = 30^0$ during melting at HTF flow of Re = 500, 1000, and 1500 at $T_{HTF} = 50$ °C.

## 4. Numerical modelling and validation

The CFD simulation is performed using ANSYS-Fluent using the QUICK scheme for the diffusion fluxes and convection and PRESTO scheme the pressure equation considering 10^{-6} for the convergence. The configuration of the mesh adopted in all computations is shown in Fig. 2. Several pre-simulation runs are conducted to ensure a mesh and time-step independence of the numerical solution. Numerical tests are primarily done with N = 34,652, 39,317 and 45,185 mesh cells as shown in Fig. 3. These tests show that the mesh of 39,317 cells is precise enough to properly describe the PCM thermofluidic behaviour during the melting and solidification processes. In a 30° zig-zag case, the difference in the liquid fraction value among the three grids is less than 1%. Further mesh refinement almost produces the same results. Therefore, the mesh of 39,317 is chosen for performing the numerical analysis. Regarding the time-step independence of the solution, three differ-

ent time steps ($\Delta t = 0.3$, 0.5 and 1 s) are used to test the consistency of the simulation scheme as shown in Fig. 3. The maximum deviations in the liquid fraction are less than 0.5% in the case of $\Delta t = 1$ s with respect to other time steps. Therefore, the analysis reported in this paper is performed on $\Delta t = 1$ s for better saving of the computational cost.

Verification of the developed FLUENT code is done via the study of Mat et al. [46], which was performed both numerically and experimentally. Mat et al. [46] analysed a fined double-tube LHSHE unit using TR58 as the PCM with constant wall temperatures as the boundary condition. They examined the presence of fins connected to both inner and outer tubes in the PCM zone in a staggered form. As shown in Fig. 4, an excellent agreement is achieved comparing the presented results with the measurements and numerical data for the temperature and numerical prediction of melt fraction from Mat et al. [46].

a) α=60⁰
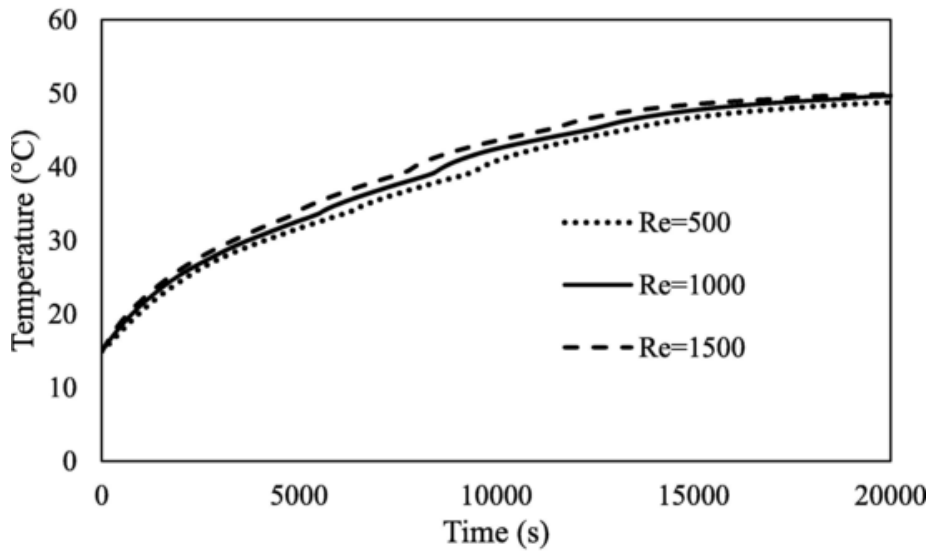
b) α=30⁰

Fig. 12. Transient variations of the PCM average temperature for th thee case with a) $\alpha = 60^\circ$ and b) $\alpha = 30^\circ$ during melting at HTF flow of $Re = 500, 1000$, and 1500 at $T_{HTF} = 50$ °C.

Table 4
Effect of applying HTF flow of different Reynolds numbers on the melting time and heat storage rate in the zigzag PCM channel.

Inlet HTF Re	Melting time (s)		Heat storage rate (W)	
	$\alpha = 30°$	$\alpha = 60°$	$\alpha = 30°$	$\alpha = 60°$
500	21,659	12,198	152.24	311.07
1000	18,784	10,430	175.63	364.82
1500	17,355	9355	190.20	406.84

5. Results and discussion

5.1. Melting mode

5.1.1. Effect of zigzag angle within the PCM channel

Four different values of zigzag angle ($\alpha = 15°$, 30°, 45° and 60°) are considered to examine the effects of zigzag angle on the PCM melting front evolution and the corresponding isotherm distribution during the melting mode. Fig. 5 shows the temporal evolution of the melting front over four different melting durations ($t = 900, 1800, 3600$, and 5400 s) at $T_{HTF} = 50$ °C. As can be seen, the melting front (represented in light yellow colour) is almost a set of straight lines parallel to the hot zigzag walls during the early duration ($t \leq 900$ s). This is because conduction which is dominated during this duration as the main heat transport mechanism between the HTF fluid flowing outside the zigzag channel and the PCM contained within it. As time proceeds, the role of
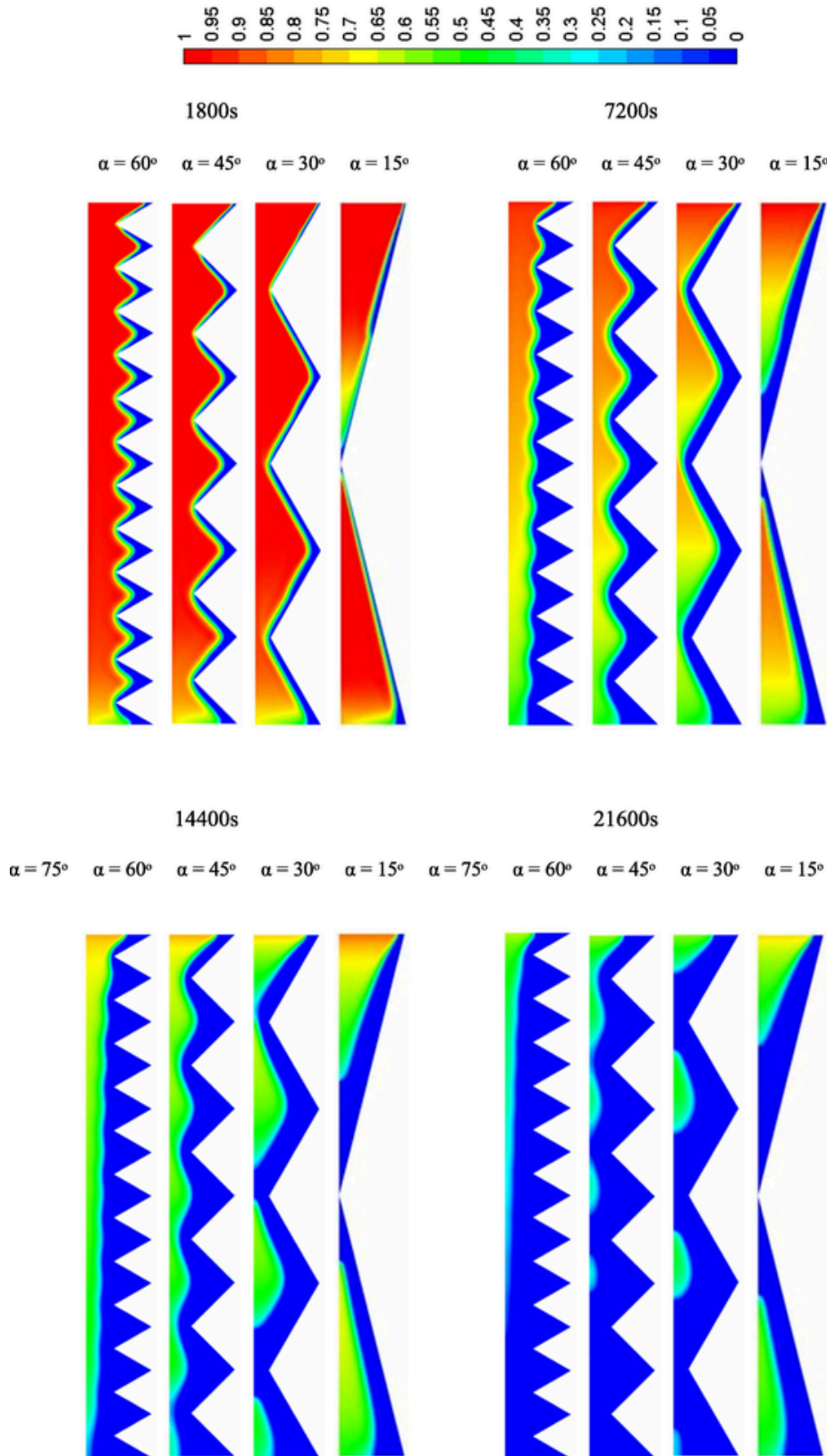
Fig. 13. Liquid-fraction contours at various time durations and various angles of zigzag configuration during the solidification of PCM at $T_{HTF} = 15$ °C.

natural convection shows up when hot part of melted PCM starts to flow in the upward direction under the effect of buoyancy. As time further proceeds, buoyancy gets more effective to induce a stronger role of natural convection, which in turn, acts as an additional heat transport supply to the melted PCM. Thus, it contributes to the quicker spread of

melting at the upper part of the PCM channel relative to the bottom. Thus, after the first hour ($t = 3600$ s), the melting front begins to slowly lose the uniform shape of the straight line. As further time elapses, the melt portion increases in size to inhabit all the PCM domain. Due to the more effective role of natural convection compared to
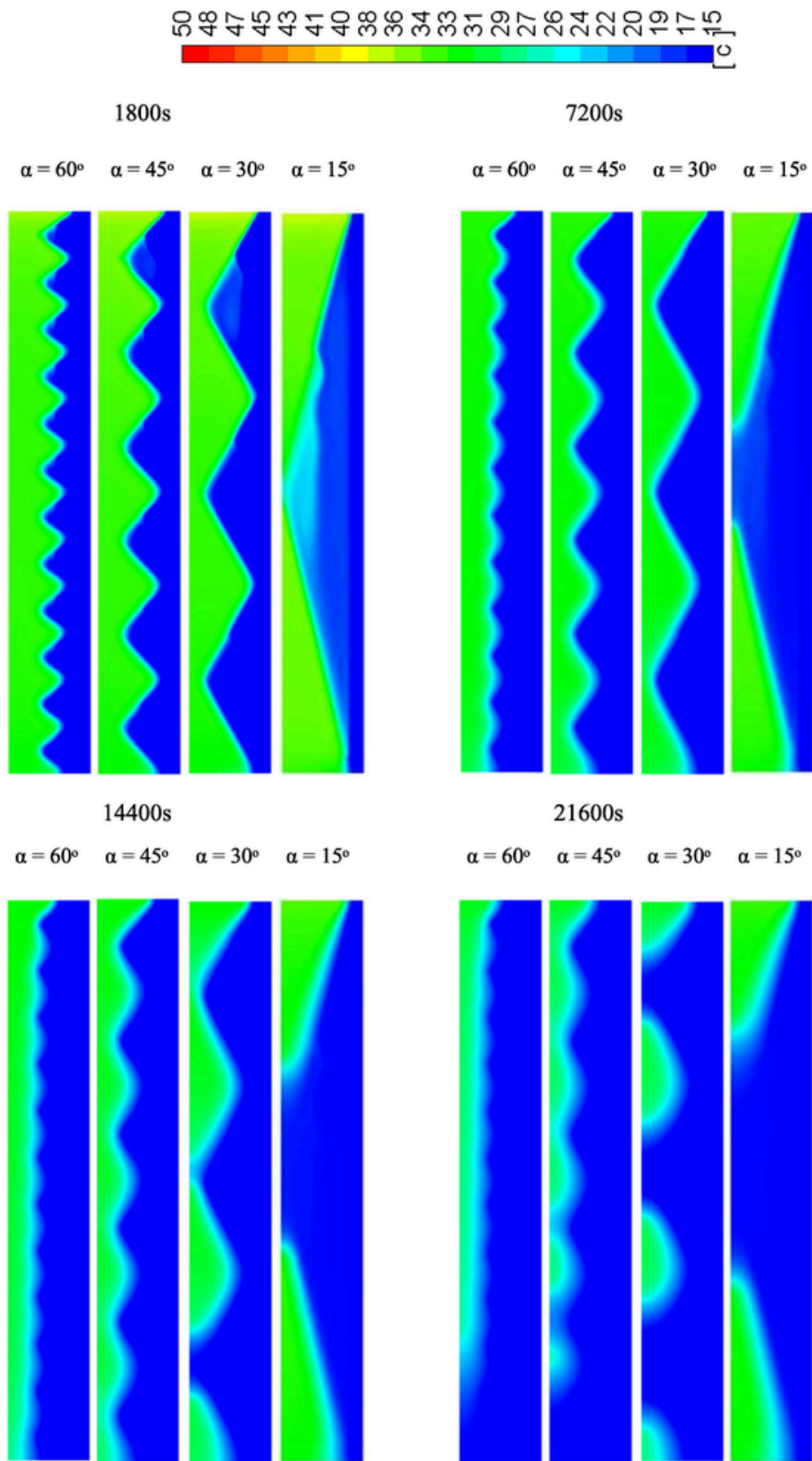
Fig. 14. Temperature contours (in °C) at various time durations and various angles of zigzag configuration during the solidification of PCM at $T_{HTF} = 15$ °C.

that of conduction, the melting terminates earlier at the upper part of the channel, as can be observed in Fig. 5 at ($t = 5400$ s). The PCM adjacent to the zigzag walls at the top melts faster due to the better natural movement (circulation) of the molten PCM which is generated due to the better density variation of the warm molten PCM compared to solid PCM. Thus, the molten PCM appears to circulate faster and reach an earlier melting termination at ($t = 5400$ s) at the top, whereas other parts take more time to reach the melting completion.
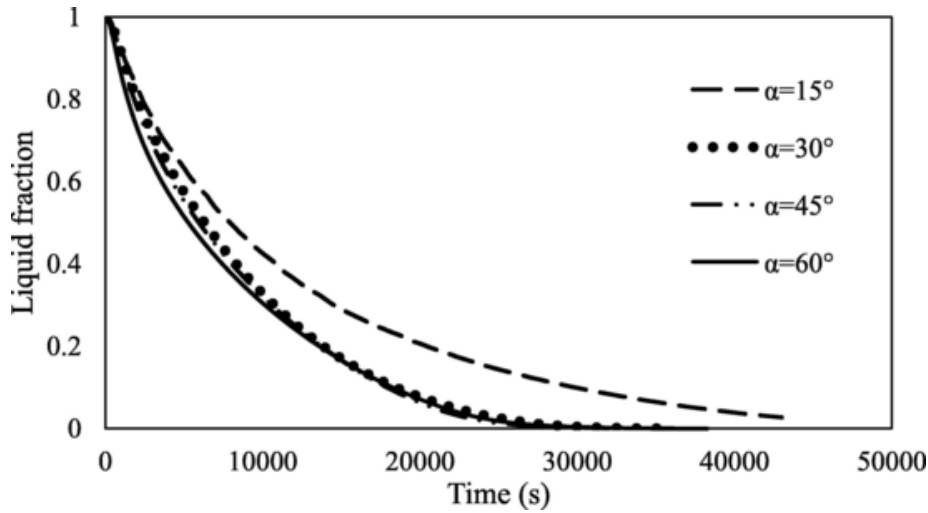
Fig. 15. Transient variations of the PCM liquid fraction during melting at the zigzag angle of α = 15°, 30°, 45°, and 60° at T_{HTF} = 15 °C.

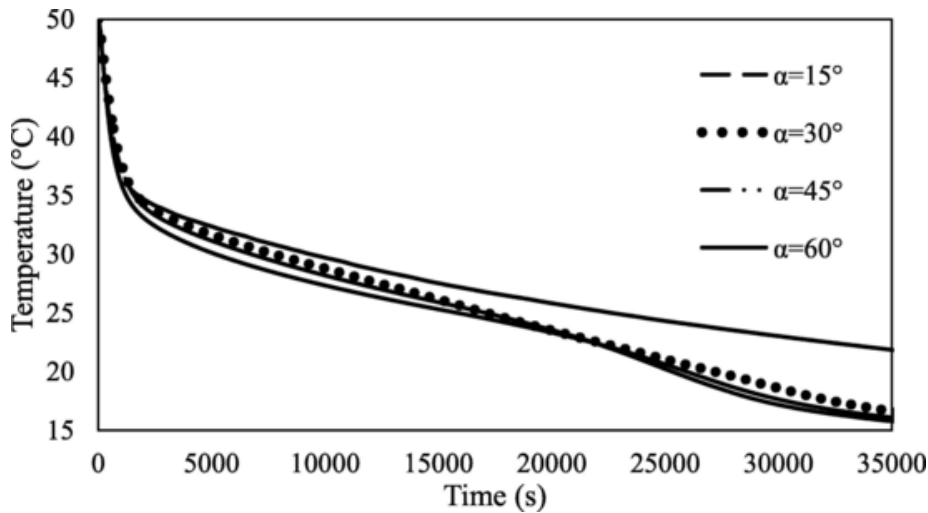**Fig. 16.** Transient variations of the average PCM temperature during melting at the zigzag angle of α = 15°, 30°, 45°, and 60° at T_{HTF} = 15 °C.

Table 5
Effect of applying different zigzag angles on the solidification time, heat retrieval capacity and heat retrieval rate in the zigzag PCM channel.

α (°)	PCM mass (kg)	Solidification time (s)	Heat retrieval capacity (J)	Heat retrieval rate (W)	ΔP (Pa)	Pumping power (W)
15	11.73	51,295	−2,612,681	−50.93	370.4	205.2
30	14.44	34,582	−3,269,750	−94.55	455.9	252.4
45	15.65	33,100	−3,560,800	−107.58	494.5	273.9
60	16.70	33,048	−3,801,880	−114.90	527.8	292.4

Concerning the impact of zigzag angle, the study predictions reveal that increase of the angle size does not post an obvious difference on the melting front location in the early durations of melting ($t \leq 900$ s), as can be seen in Fig. 5. This is attributable to the nature of flow-resistant forces invoked by the zigzag alignment of the PCM channel that can highly suppress the role of natural convection. Moreover, increasing the size of the zigzag angle increases the proportion of melted PCM as can be observed in comparing the case of 60°- zigzag angle with other cases. These differences are more obvious during the final intervals due to the larger heat-exchange area in the case of 60°- zigzag angle compared to other cases. For example, at t = 5400 s there is still a portion of PCM not melted (marked in blue colour) at (α = 15°), whereas the size of this portion is much smaller at (α = 60°). Hence, the

impact of zigzag configuration on the melting front evolution becomes more discernible as time elapses and/or zigzag angle size increases.

Fig. 6 shows temperature contours over different periods of melting for the cases of zigzag angles of (α = 15°,30°, 45° and 60°) at T_{HTF} = 50 °C. During the earliest period ($t \leq 900$ s), the heat transfer occurring between the hot walls of the PCM channel and not melted PCM is largely dominated by conduction rather than natural convection. Therefore, the isotherms look like a series of straight lines during this period. It would be worthy to mention here that both natural convection and thermal conduction affect the temperature of the PCM, but the role of conduction is dominant during the early period. However, the isotherms begin to depart from the uniformity in shape as time goes on to the next periods of melting ($t \geq 1800$ s). A series of rotating cells begin to display as a sign of initiating a significant contribution of convection in the heat transfer process. Throughout these periods, the rotating cells look bigger and more deformed in shape within the melting zone owing to the effective role of convection. This can be seen by comparing the isotherms between the time periods considered (1800 s, 3600 s and 5400 s), as shown in Fig. 6.

The transient evolution of the PCM liquid-fraction profiles and the average temperature profiles are depicted in Figs. 7 and 8, respectively. It can be realized that a larger liquid fraction and larger average temperature are generally generated by increasing the size of the zigzag angle in use. The data from Figs. 7 and 8 which is also summarized in
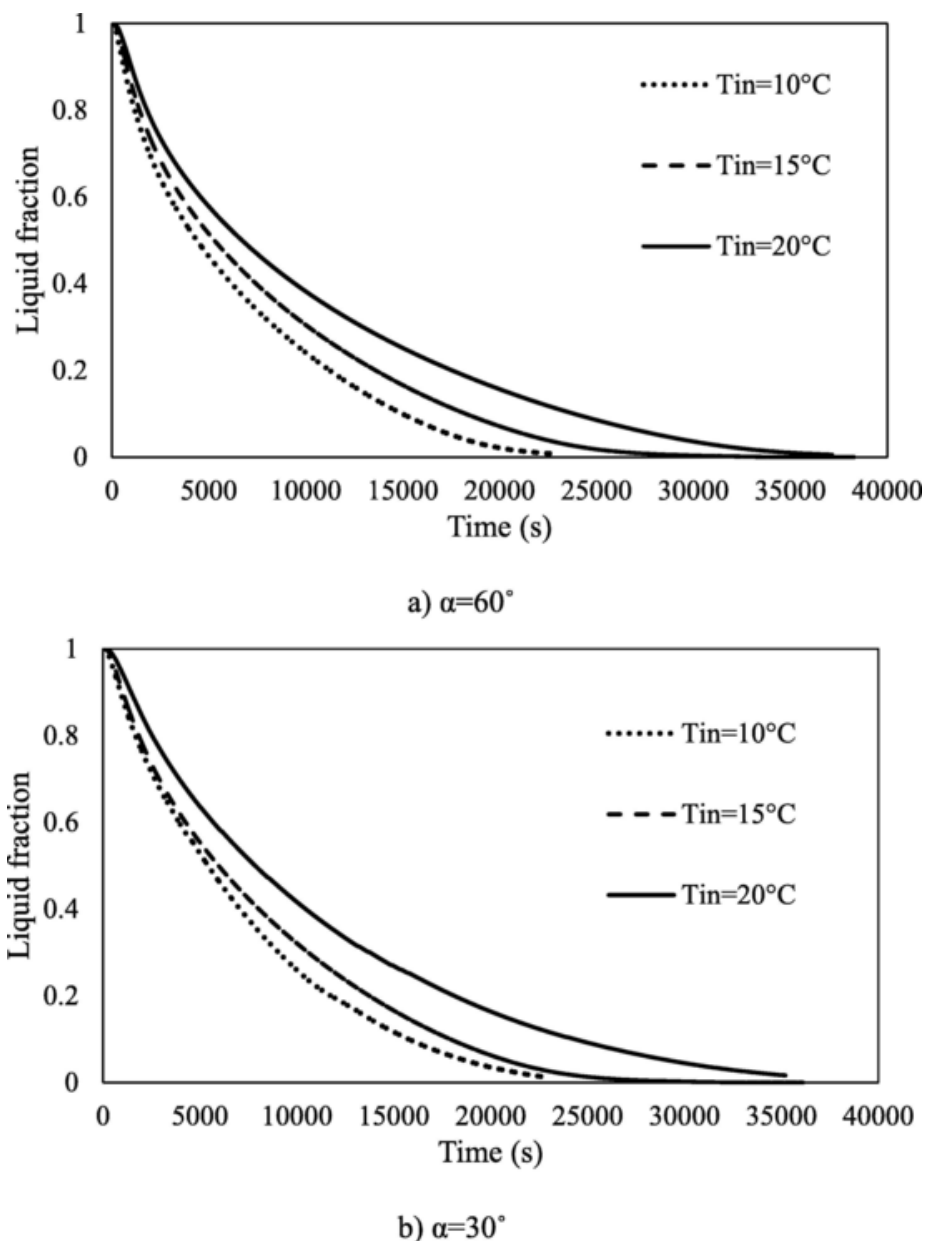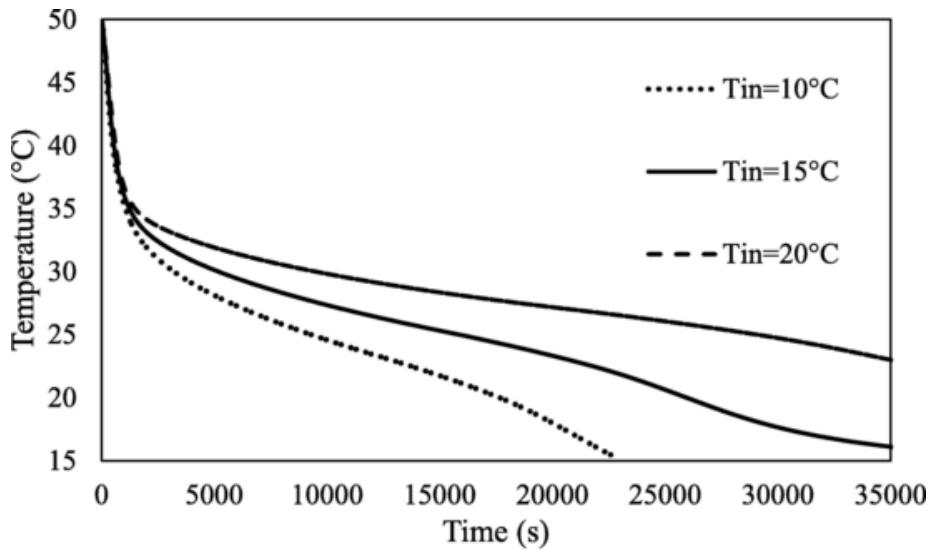
a) α=60˚

b) α=30˚

Fig. 17. Transient variations of the PCM liquid fraction for the cases with a) α = 60˚ and b) α = 30˚ during solidification at T_{HTF} = 10, 15, and 20 ˚C.

Table 2 which indicates that applying higher zigzag angle can always lead to faster melting rate and shorter duration to reach the status of complete melting. During the melting duration, the 60˚-zigzag angle preserves superior melting performance among all the angles considered in terms of liquid-fraction profile, average temperature profile, and total melting time. According to Table 3, applying a zigzag angle of 60˚ results in the best melting rate as the PCM completes the melting within 10,429 s, whereas the complete melting requires 11,224 and 18,184 s in the other cases of 45˚- and 30˚- zigzag angle, respectively. Taking the reference to 30˚, the results from Table 2 show that the melting rate could be improved by 38.3% and 42.6% with the application of 45˚ and 60˚ angle, respectively. In short, the application of higher zigzag angles results in a higher melting rate, thereby the potential of the PCM channel to handle the energy storage duties becomes more stabilized.

The predicted values of thermal storage capacity and thermal storage rate for the three different zigzag angles considered are also listed in Table 2. The amount of thermal storage capacity generally increases with the use of a higher zigzag angle. This is attributed to the fact that

a larger amount of PCM can be accommodated in the zigzag channel if a larger zigzag angle is applied. For example, applying the zigzag angle of 60˚ can increase the energy storage capacity up to 13.8% compared to that of the reference case of 30˚ angle. Meanwhile, the use of a higher zigzag angle assists higher thermal storage rate to arise. As can be seen from Table 2, applying the zigzag angle of 60˚ would raise the storage rate by 98.3% compared to that of the reference case of 30˚ angle. The reason is that the use of the higher zigzag angle of 60˚ can also increase the rate of heat transfer due to the larger heat-exchange area associated with large zigzag angles. Therefore, the use of a larger zigzag angle is advantageous in both aspects of the thermal storage capacity and the thermal storage rate. Furthermore, it should be noted that as presented in Table 2, the difference between the performance of the system for the cases with the orientation angles of 45˚ and 60˚ is less than that for the orientation angles of 15˚ and 30˚. Therefore, it can be concluded that by increasing the orientation angle more than 60˚, the performance of the system negatively decreases.

However, the use of high zigzag angles can also negatively increase the pumping power consumption in the HTF side. As presented in Table

a) α=60˚
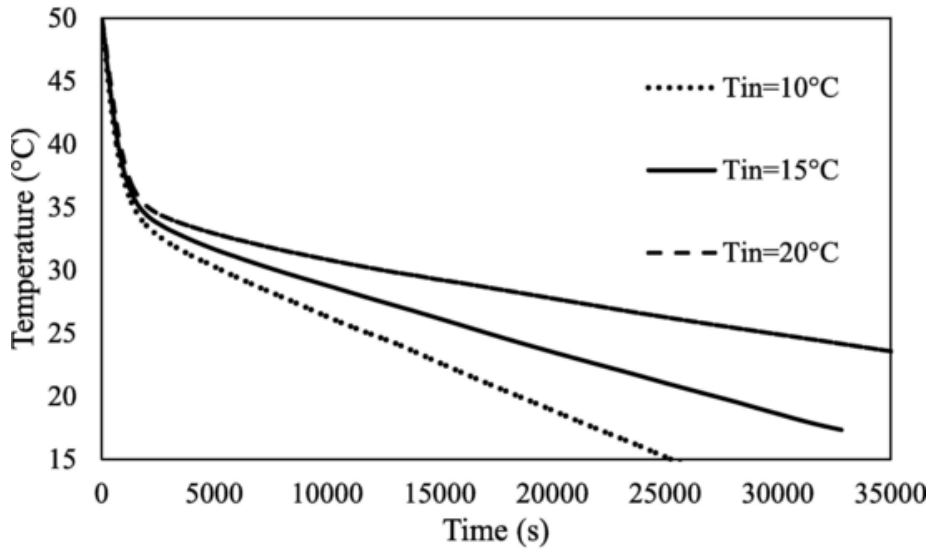
b) α=30˚

Fig. 18. Transient variations of the PCM average temperature for the cases with a) α = 30˚ and b) α = 30˚ during solidification at T_{HTF} = 10, 15, and 20 ˚C.

Table 6

Effect of applying different HTF inlet temperature on the solidification time and heat retrieval rate in the zigzag PCM channel.
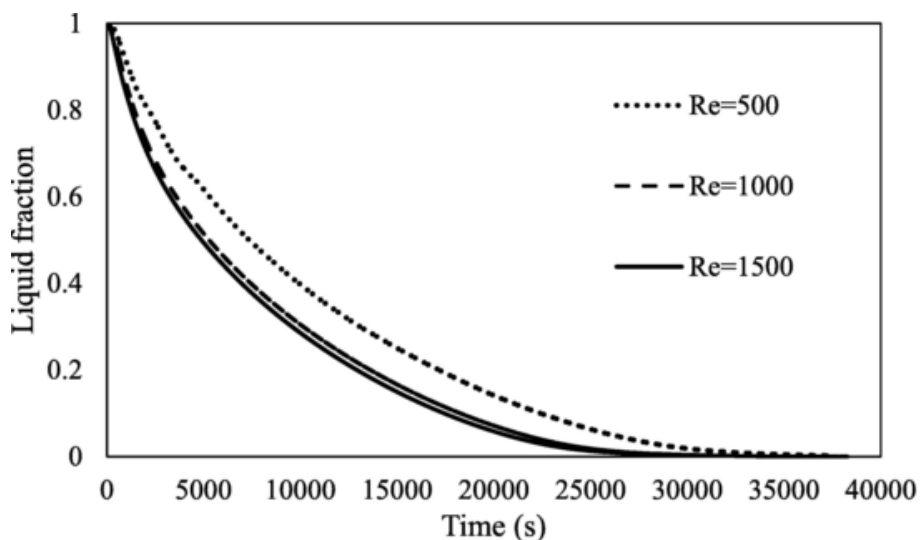
Inlet HTF temperature (˚C)	Solidification time (s)		Heat retrieval rate (W)	
	α = 30˚	α = 60˚	α = 30˚	α = 60˚
10	28,716	27,802	−117.82	−137.14
15	34,582	34,848	−94.55	−109.10
20	43,917	41,562	−70.62	−86.22

2, the use of a larger zigzag angle results in a higher pressure drop and leads to larger consumption of pumping power according to Eq. (9). Therefore, the gain obtained from increasing the zigzag angle in the melting enhancement of PCM is accompanied by an inevitable cost of the pressure-drop rise, which results from increasing of friction with the walls of the zigzag plates as the orientation angle increases. In summary, increasing the orientation angle within the range of 15˚ to 60˚ can significantly improve the storage performance of the system, but also the cost of pumping power is negatively increasing. Therefore, it should be there proper selection of the zigzag angle orientation to ensure good storage performance of the PCM within minimal pumping power consumption by the HTF.

5.1.2. Effect of inlet HTF temperature

Three different values of inlet HTF temperature of (T_{HTF} = 45, 50 and 55 ˚C) are considered to examine the influence of HTF temperature on the development of the liquid-fraction profile and average temperature profile in Figs. 9 and 10, respectively. The data from figures indicates that the duration of melting is shorter, and the average PCM temperature is higher as the inlet HTF temperature is higher. That is attributable to the fact that a higher inlet HTF temperature assists a larger temperature difference with reference to the PCM melting point, thereby a faster PCM melting rate and then greater PCM temperature arises. The data from Table 3 shows that the PCM at α = 60˚ requires

a) α=60˚
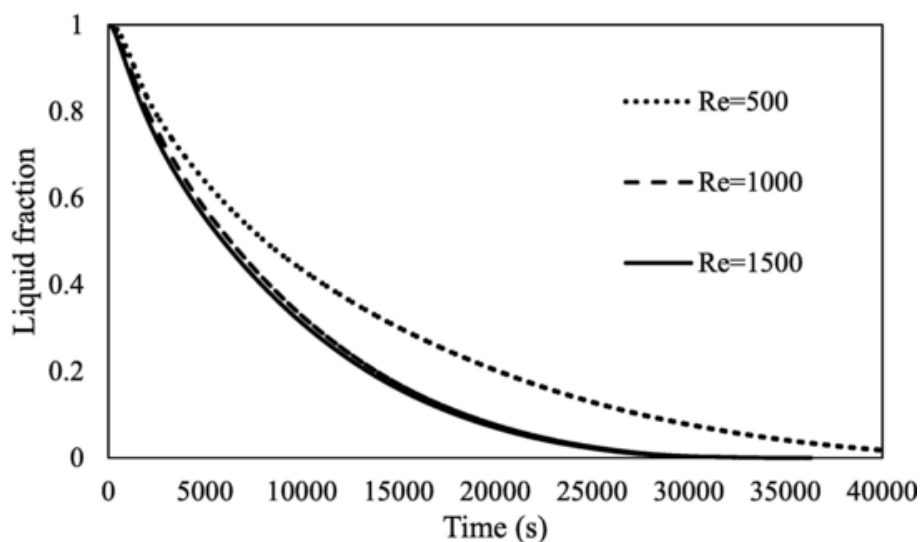
b) α=30˚

Fig. 19. Transient variations of the PCM liquid fraction for the cases with a) α = 60˚ and b) α = 30˚ during solidification at HTF flow of Re = 500, 1000 and 1500.

14,081 s to complete the melting phase at the HTF temperature of 45 ˚C. Also, it does require 10,430 and 8685 s to complete the melting for HTF temperature at 50 and 55 ˚C, respectively. This means that, when the HTF temperature is raised from 45 to 50 ˚C and 55 ˚C, the overall melting time can be saved by about 25.9% and 38.3%, respectively. Concerning the impact of the HTF temperature on the thermal storage rate, Table 3 shows that due to the increase of the HTF temperature from 45 to 50 ˚C and 55 ˚C, the thermal storage rate in the case of α = 60˚ can be increased from 260.70 to 364.82, and 455.16 W, respectively. This is about 39.8% and 74.6% higher storage rate, respectively. This indicates that the potential of zigzag configuration for the thermal performance improvement increases as the HTF inlet temperature increases. This would also imply that it is necessary to optimize the zigzag angle arrangement with the values of inlet HTF temperature to ensure the best possible melting enhancement.

5.1.3. Effect of HTF Reynolds number

Reynolds number (Re) for the flowing HTF outside the PCM channel varies according to the relation ($Re = 4\dot{m}/(\pi D \mu)$), where ($\dot{m}$) is the change of mass flowrate of water as the HTF, μ is the dynamic viscosity of water at $T = 50$ ˚C, and D is the diameter of the HTF channel. Three different values ($Re = 500, 1000,$ and 1500) are considered to investigate the impact of the HTF Reynolds number on the evolution of liquid-fraction profile and average temperature profile in Figs. 11 and 12, respectively. The data from figures indicate that the average PCM temperature and liquid fraction are higher as the Reynolds number is higher. This is because higher Reynolds numbers (higher flowrates) promote better coefficient of convective heat transfer on the zigzag surface, which results in a higher heat transport rate between the HTF and PCM. The data listed in Table 4 shows that the PCM at α = 60˚ requires 12,198 s to finish melting at $Re = 500$. However, it does require 10,430 and 9355 s to finish melting for HTF flow at $Re = 1000$ and 1500, respectively. This means that, when the

a) α=60°
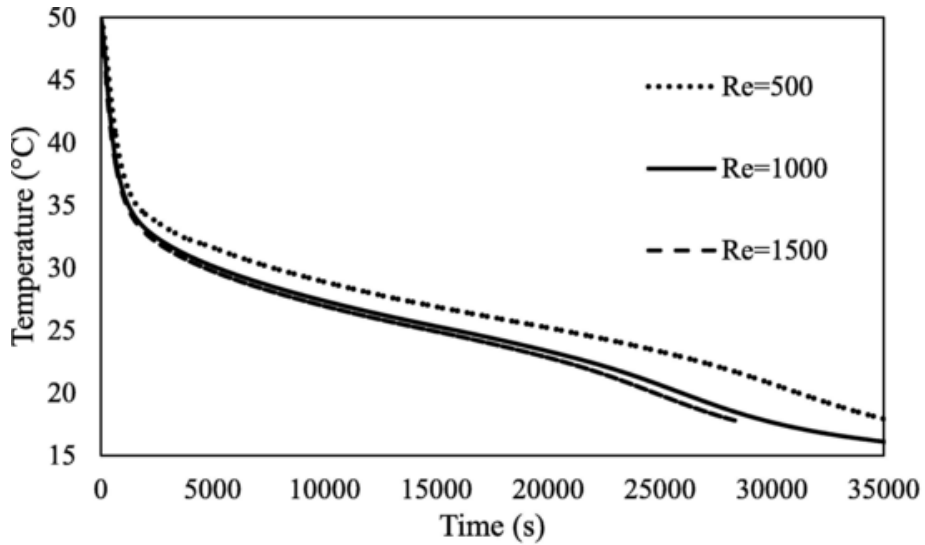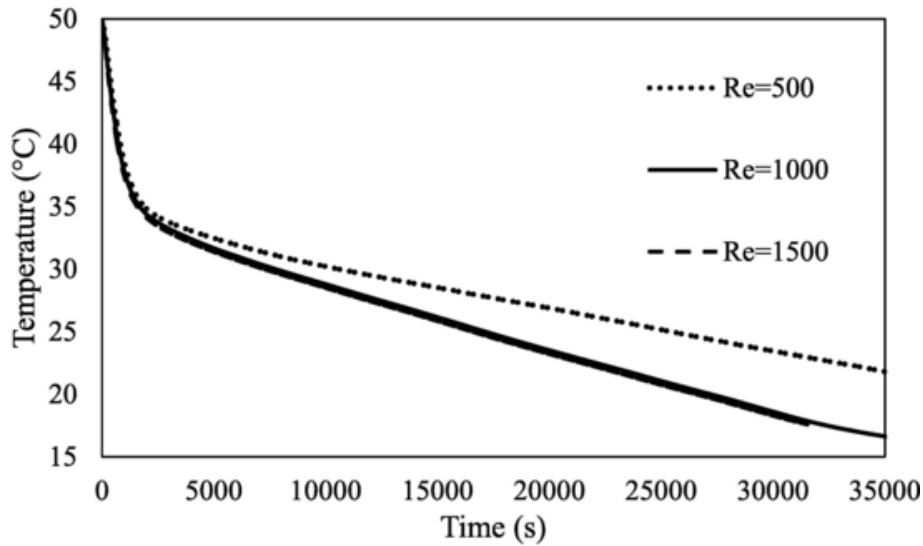
b) α=30°

Fig. 20. Transient variations of the PCM average temperature for the cases with a) α = 60° and b) α = 30° during solidification at Re = 500, 1000 and 1500.

Table 7
Effect of applying HTF flow of different Reynolds numbers on the solidification time and heat retrieval rate in the zigzag PCM channel.

Inlet HTF Re	Solidification time (s)		Heat retrieval rate (W)	
	α = 30°	α = 60°	α = 30°	α = 60°
500	48,783	39,656	−65.56	−95.00
1000	34,582	34,848	−94.55	−109.10
1500	33,737	32,308	−96.09	−115.61

Re of HTF flow is raised from 500 to 1000 and 1500, the overall time for melting can be reduced by about 14.6% and 23.3%, respectively. Concerning the impact of Re of the HTF flow on the thermal storage rate, Table 4 shows that due to the increase of Re from 500 to 1000 and 1500, the thermal storage rate can be increased from 311.07 to 364.82 and 406.84 W, respectively. This means 17.3% and 30.8% higher storage rate, respectively. This implies that the enhancement capacity of zigzag configuration increases as Re of the HTF flow in-

creases. This trend would also imply that applying zigzag angle needs to be adjusted with the values of HTF flowrate to guarantee the best possible melting performance.

5.2. Solidification

5.2.1. Effect of zigzag angle within the PCM channel

Four different values of zigzag angle (α = 15°, 30°, 45° and 60°) are considered to demonstrate the effects of zigzag angle on the PCM melting front evolution and the corresponding isotherm distribution during the melting mode. Fig. 13 shows the temporal evolution of the solidification front over four different periods of solidification (t = 1800, 7200, 14,400, and 21,600 s) at T_{HTF} = 15 °C. During the initial stage (t ≤ 1800 s), the solidification front (shown in light green colour) takes the shape of the thick curved line parallel to the zigzag walls. This is due to the heat release from the not solidified PCM to the zigzag cold walls adjacent to the HTF is mainly managed by heat conduction mode. Increasing the zigzag angle during this period causes no sound

impact on the position of the solidification front since only a thin solidified layer could be established during this period. As time proceeds ($t = 7200$ s), a weak role of natural convection shows up when some melted PCM starts to move in the ascendant direction under the effect of buoyancy. However, the buoyancy is not that influential enough to produce a sound deformation in the shape of the solidification front. Therefore, solidification fronts get thicker and start to change their locations away from the zigzag walls because of the dominant role conduction over natural convection across the PCM. As further time elapses, the solidified portion increases in size to inhabit the major area of the PCM domain. Due to the dominating role of natural convection compared to that of conduction, the solidification ends early at the lower part of the PCM domain in all cases considered, as can be observed at ($t = 21,600$ s) in Fig. 13.

Fig. 14 shows temperature contours over different durations of solidification for the cases of zigzag angles of ($\alpha = 15°, 30°, 45°$ and $60°$) at $T_{HTF} = 15$ °C. During the earliest period ($t \leq 1800$ s), the heat transfer occurring between the cold walls of the PCM channel and liquid PCM is largely dominated by conduction rather than natural convection. Therefore, the isotherms look like a series of straight lines during this period. It would be worthy to mention here that both natural convection and thermal conduction affect the temperature of the PCM, but the role of heat conduction remains the most influential during the initial solidification stage. However, the isotherms begin to depart from the uniformity in shape as time goes on to the next periods of solidification ($t \geq 7200$ s). Throughout these periods, the increase of zigzag angle shows effective change on the shape and position of the solidification fronts due to the larger heat transfer rate owing to the larger heat-exchange area in addition to the relatively prominent role of the convection. In the final period ($t \geq 21,600$ s), the solidified layer grows to cover the major portion of the PCM domain as can be seen by comparing the isotherms between the four cases of ($\alpha = 15°, 30°, 45°$ and $60°$) in Fig. 14.

Figs. 15 and 16 compares the transient evolution of the liquid-fraction and the average temperature profiles at four different zigzag angles ($\alpha = 15, 30°, 45°$ and $60°$), respectively. It can be realized that a slightly larger fraction of liquid PCM and a higher average temperature is created due to increasing the size of the used zigzag angle. The data from the figures which is also summarized in Table 5 indicates that applying higher zigzag angle can lead to faster solidification rate and shorter duration of solidification. During the solidification duration, the 60°-zigzag angle preserves superior solidification performance among all the angles considered in terms of liquid-fraction profile, average temperature profile, and total solidification time. According to Table 5, applying a zigzag angle of 60° results in the best solidification rate as the PCM completes the solidification within 34,582 s, whereas the complete solidification requires 33,100 and 33,048 s in the other cases of 45°- and 30°- zigzag angle, respectively. Taking the reference to 30°, the results from Table 5 show that the solidification rate could be improved by 4.1% and 4.4% with the application of 45 and 60 zigzag angles, respectively. In short, the application of higher zigzag angles results in a higher solidification rate, thereby the potential of the PCM channel to handle the energy retrieval duties becomes more stabilized. Also, it can be seen from Table 5 that applying zigzag angle of 60° would raise the heat retrieval capacity 16.3% and the heat retrieval rate 21.4% compared to that of the reference case of 15° angle. In general, the solidification rate of PCM is faster and the heat retrieval rate is higher with higher zigzag angle. The reason is that the use of higher zigzag angle can also increase the rate of heat transfer due to the larger heat-exchange area so that better solidification evolution occurs through the PCM domain.

5.2.2. Effect of inlet HTF temperature

The influence of the inlet HTF temperature on the temporal evolution of liquid-fraction profile and the average temperature profile was analyzed at three different values of HTF inlet temperature ($T_{HTF} = 10$, 15 and 20 °C) as shown in Figs. 17 and 18, respectively. The figures show that the solidification duration is shorter and the average PCM temperature is lower as the HTF temperature is lower. This is because employing of a lower HTF inlet temperature helps make a greater difference in temperature in relative to the PCM solidifying point, thereby a quicker PCM solidifying rate is resulting with lower average PCM temperature. Table 6 data shows that the PCM in the case of $\alpha = 60°$ takes only 27,802 s to complete the solidification process at 10 °C of inlet HTF temperature. However, the PCM at HTF temperatures of 15 and 20 °C requires 34,848 and 41,562 s for the solidification completion, respectively. This indicates that the solidification period can be saved by around 20.2 and 33.1% respectively if the HTF temperature is decreased from 20 to 15 °C and 10 °C. Data from Table 6 also reveals that the heat retrieval rate can be improved from −86.22 to −109.10 and −137.14 W due to the decrease of the HTF temperature from 20 to 15 °C and 10 °C, respectively. This represents an increase in the retrieval rate by about 25.7% and 59.1%, respectively. Therefore, it can be concluded the potential of zigzag channel for improving the solidification behavior of PCM improves with decreasing the inlet HTF temperature. Thus, optimizing the selection of zigzag angle orientation should also be depending on the inlet HTF temperature values to ensure superior solidification performance of PCM.

5.2.3. Effect of HTF Reynolds number

To show the effect of HTF Reynolds number on the evolution of the liquid fraction profile and average temperature profile, three different values (Re = 500, 1000, and 1500) are undertaken for the study as shown in Figs. 19 and 20, respectively. The data from these figures show that, as the Reynolds number increases from 500 to 1500, the PCM solidification time and average temperature both decreases. This is attributable to the fact that higher flow rates of HTF (higher Re) facilitate a stronger heat transfer by convection on the zigzag plate, thus higher heat transport rates between HTF and PCM are generated. The data in Table 7 show that 39,656 s are needed for PCM to complete solidification at Re = 500 in the case of $\alpha = 60°$. However, the solidification completion at Re = 1000 and 1500 needs 34,848 and 32,308 s, respectively. This indicates that the solidification duration of PCM can be shortened by about 13.8% and 22.7% if the Re of the HTF flow is increased from 500 to 1000 and 1500, respectively. With regard to the effect of Re in the HTF flow on thermal retrieval rate, the data in Table 7 also reveals that the thermal retrieval rate can be increased from 95.0 W to 109.1 and 115.6 W when the Re increases from 500 to 1000 and 1500, respectively. This means a higher retrieval rate of 12.9% and 17.8%, respectively. Therefore, it can be summarized that the capability of zigzag plate configuration on improving the storage performance of PCM increases as the Re of the HTF flow increases. This outcome also means that the orientation of zigzag angle must be optimized with the HTF flowrate to ensure the best possible solidification rate enhancement.

6. Conclusions

Surface interruption via zigzag configuration is proposed in this study for better enhancement in the heat storage performance of PCM contained in horizontal channels. The impact of three different zigzag angles along with several values of flow temperature and mass flowrate of the heat-transfer fluid (HTF) during the consecutive charging and discharging is numerically examined and validated via related previous studies. The conclusions from this study can be summarized as:

(1) Increasing the size of zigzag angle does not post a very much difference in the evolution of melting or solidification during their earlier durations. However, the impact of zigzag angle

configuration on the melting and solidification evolution becomes more discernible as time elapses and/or zigzag angle size increases.

(2) Larger size of zigzag angle results in a higher melting rate, larger thermal storage capacity, and higher storage rate thus the potential of the PCM channel to handle the energy storage duties becomes more stabilized.

(3) Higher flow temperature of the HTF assists a higher temperature difference relative to the PCM melting point, thereby faster PCM melting and solidifying rates are accomplished. This would imply that it is necessary to optimize the zigzag angle arrangement with the inlet HTF temperature to ensure the best possible enhancement in the thermal response of PCMs.

(4) Faster melting and solidification rates can be achieved as higher Reynolds number of the HTF flow is applied since higher Reynolds numbers (higher flowrates) promote better coefficient of convective heat transfer on the zigzag wall, which results in higher heat transport rate between the HTF and PCM.

(5) The melting and heat storage rates of PCM are higher with higher zigzag angles. The melting rate could be improved by 38.3% and the heat storage rate increased by 74.6% with increasing the zigzag angle from 15° to 60°. Also, the solidification and heat retrieval rates are higher with higher zigzag angles. An improvement of about 16.3% and 21.4% can be achieved in the solidification rate and retrieval respectively with increasing the zigzag angle from 15° to 60°.

Declaration of Competing Interest

The authors declare that they have no known competing financial interests or personal relationships that could have appeared to influence the work reported in this paper.

References

[1] F. Martins, C. Felgueiras, M. Smitkova, N. Caetano, Analysis of fossil fuel energy consumption and environmental impacts in European countries, Energies 12 (2019) 964.

[2] S.D. Cîrstea, C. Moldovan-Teselios, A. Cîrstea, A.C. Turcu, C.P. Darab, Evaluating Renewable Energy Sustainability by Composite Index, Sustainability. 10 (2018) 811.

[3] N.I. Ibrahim, F.A. Al-Sulaiman, S. Rahman, B.S. Yilbas, A.Z. Sahin, Heat transfer enhancement of phase change materials for thermal energy storage applications: A critical review, Renew. Sustain. Energy Rev. 74 (2017) 26–50.

[4] J.M. Mahdi, S. Lohrasbi, E.C. Nsofor, Hybrid heat transfer enhancement for latent-heat thermal energy storage systems: A review, Int. J. Heat Mass Transf. 137 (2019) 630–649.

[5] D. Fernandes, F. Pitié, G. Cáceres, J. Baeyens, Thermal energy storage:"How previous findings determine current research priorities", Energy. 39 (2012) 246–257.

[6] H. Cui, X. Yuan, X. Hou, Thermal performance analysis for a heat receiver using multiple phase change materials, Appl. Therm. Eng. 23 (2003) 2353–2361.

[7] M. Fang, G. Chen, Effects of different multiple PCMs on the performance of a latent thermal energy storage system, Appl. Therm. Eng. 27 (2007) 994–1000.

[8] Z.-X. Gong, A.S. Mujumdar, Cyclic heat transfer in a novel storage unit of multiple phase change materials, Appl. Therm. Eng. 16 (1996) 807–815.

[9] Z. Hu, A. Li, R. Gao, H. Yin, Enhanced heat transfer for PCM melting in the frustum-shaped unit with multiple PCMs, J. Therm. Anal. Calorim. 120 (2015) 1407–1416.

[10] R. Seeniraj, N.L. Narasimhan, Performance enhancement of a solar dynamic LHTS module having both fins and multiple PCMs, Sol. Energy 82 (2008) 535–542.

[11] P. Wang, D. Li, Y. Huang, X. Zheng, Y. Wang, Z. Peng, et al., Numerical Study of Solidification in a Plate Heat Exchange Device with a Zigzag Configuration Containing Multiple Phase-Change-Materials, Energies 9 (2016) 394.

[12] J.M. Mahdi, H.I. Mohammed, E.T. Hashim, P. Talebizadehsardari, E.C. Nsofor, Solidification enhancement with multiple PCMs, cascaded metal foam and nanoparticles in the shell-and-tube energy storage system, Appl. Energy 257 (2020) 113993.

[13] J.C. Kurnia, A.P. Sasmito, S.V. Jangam, A.S. Mujumdar, Improved design for heat transfer performance of a novel phase change material (PCM) thermal energy storage (TES), Appl. Therm. Eng. 50 (2013) 896–907.

[14] S. Mehryan, M. Vaezi, M. Sheremet, M. Ghalambaz, Melting heat transfer of

[15] power-law non-Newtonian phase change nano-enhanced n-octadecane-mesoporous silica (MPSiO2), Int. J. Heat Mass Transf. 151 (2020) 119385.

[16] M. Izadi, M. Ghalambaz, S. Mehryan, Location impact of a pair of magnetic sources on melting of a Magneto-Ferro phase change substance, Chin. J. Phys. (2020).

[17] S. Mehryan, A. Tahmasebi, M. Izadi, M. Ghalambaz, Melting behavior of phase change materials in the presence of a non-uniform magnetic-field due to two variable magnetic sources, Int. J. Heat Mass Transf. 149 (2020) 119184.

[18] M. Ghalambaz, J. Zhang, Conjugate solid-liquid phase change heat transfer in heatsink filled with phase change material-metal foam, Int. J. Heat Mass Transf. 146 (2020) 118832.

[19] A. Veismoradi, A. Modir, M. Ghalambaz, A. Chamkha, A phase change/metal foam heatsink for thermal management of battery packs, Int. J. Therm. Sci. 157 (2020) 106514.

[20] Y. Zhang, A. Faghri, Heat transfer enhancement in latent heat thermal energy storage system by using the internally finned tube, Int. J. Heat Mass Transf. 39 (1996) 3165–3173.

[21] K. Ismail, C. Alves, M. Modesto, Numerical and experimental study on the solidification of PCM around a vertical axially finned isothermal cylinder, Appl. Therm. Eng. 21 (2001) 53–77.

[22] A. Erek, Z. İlken, M.A. Acar, Experimental and numerical investigation of thermal energy storage with a finned tube, Int. J. Energy Res. 29 (2005) 283–301.

[23] M.K. Rathod, J. Banerjee, Thermal performance enhancement of shell and tube Latent Heat Storage Unit using longitudinal fins, Appl. Therm. Eng. 75 (2015) 1084–1092.

[24] A. Sciacovelli, F. Gagliardi, V. Verda, Maximization of performance of a PCM latent heat storage system with innovative fins, Appl. Energy 137 (2015) 707–715.

[25] D. Zhao, G. Tan, Numerical analysis of a shell-and-tube latent heat storage unit with fins for air-conditioning application, Appl. Energy 138 (2015) 381–392.

[26] W.-W. Wang, L.-B. Wang, Y.-L. He, Parameter effect of a phase change thermal energy storage unit with one shell and one finned tube on its energy efficiency ratio and heat storage rate, Appl. Therm. Eng. 93 (2016) 50–60.

[27] A. Pizzolato, A. Sharma, K. Maute, A. Sciacovelli, V. Verda, Design of effective fins for fast PCM melting and solidification in shell-and-tube latent heat thermal energy storage through topology optimization, Appl. Energy 208 (2017) 210–227.

[28] J.M. Mahdi, E.C. Nsofor, Melting enhancement in triplex-tube latent thermal energy storage system using nanoparticles-fins combination, Int. J. Heat Mass Transf. 109 (2017) 417–427.

[29] J.M. Mahdi, S. Lohrasbi, D.D. Ganji, E.C. Nsofor, Accelerated melting of PCM in energy storage systems via novel configuration of fins in the triplex-tube heat exchanger, Int. J. Heat Mass Transf. 124 (2018) 663–676.

[30] J.M. Mahdi, E.C. Nsofor, Solidification enhancement of PCM in a triplex-tube thermal energy storage system with nanoparticles and fins, Appl. Energy 211 (2018) 975–986.

[31] J.M. Mahdi, S. Lohrasbi, D.D. Ganji, E.C. Nsofor, Simultaneous energy storage and recovery in the triplex-tube heat exchanger with PCM, copper fins and Al2O3 nanoparticles, Energy Convers. Manage. 180 (2019) 949–961.

[32] H. Shokouhmand, B. Kamkari, Numerical simulation of phase change thermal storage in inclined double-pipe heat exchanger, Applied Mechanics and Materials: Trans Tech Publ, 2012, pp. 742–746.

[33] M. Hosseini, M. Rahimi, R. Bahrampoury, Thermal analysis of PCM containing heat exchanger enhanced with normal annular fins, Mech. Sci. 6 (2015) 221.

[34] X. Yang, Z. Lu, Q. Bai, Q. Zhang, L. Jin, J. Yan, Thermal performance of a shell-and-tube latent heat thermal energy storage unit: Role of annular fins, Appl. Energy 202 (2017) 558–570.

[35] Y. Yuan, X. Cao, B. Xiang, Y. Du, Effect of installation angle of fins on melting characteristics of annular unit for latent heat thermal energy storage, Sol. Energy 136 (2016) 365–378.

[36] J.C. Choi, S.D. Kim, Heat-transfer characteristics of a latent heat storage system using MgCl2· 6H2O, Energy. 17 (1992) 1153–1164.

[37] P. Wang, X. Wang, Y. Huang, C. Li, Z. Peng, Y. Ding, Thermal energy charging behaviour of a heat exchange device with a zigzag plate configuration containing multi-phase-change-materials (m-PCMs), Appl. Energy 142 (2015) 328–336.

[38] G.M. Hobold, A.K. Da Silva, Critical phenomena and their effect on thermal energy storage in supercritical fluids, Appl. Energy 205 (2017) 1447–1458.

[39] I. Sarbu, C. Sebarchievici, A comprehensive review of thermal energy storage, Sustainability. 10 (2018) 191.

[40] E. Assis, L. Katsman, G. Ziskind, R. Letan, Numerical and experimental study of melting in a spherical shell, Int. J. Heat Mass Transf. 50 (2007) 1790–1804.

[40] GmbH RT. RT35 data sheet.

[41] P. Talebizadeh Sardari, G.S. Walker, M. Gillott, D. Grant, D. Giddings, Numerical modelling of phase change material melting process embedded in porous media: Effect of heat storage size, Proc. Inst. Mech. Eng., Part A: J. Power Energy. 957650919862974 (2019).

[42] J.M. Mahdi, E.C. Nsofor, Melting enhancement in triplex-tube latent heat energy storage system using nanoparticles-metal foam combination, Appl. Energy 191 (2017) 22–34.

[43] A. Alhusseny, N. Al-Zurfi, A. Nasser, A. Al-Fatlawi, M. Aljanabi, Impact of

using a PCM-metal foam composite on charging/discharging process of bundled-tube LHTES units, Int. J. Heat Mass Transf. 150 (2020) 119320.

[44] A. Shahsavar, A. Goodarzi, H.I. Mohammed, A. Shirneshan, P. Talebizadehsardari, Thermal performance evaluation of non-uniform fin array in a finned double-pipe latent heat storage system, Energy. 193 (2020) 116800.

[45] P.T. Sardari, D. Grant, D. Giddings, G.S. Walker, M. Gillott, Composite metal foam/PCM energy store design for dwelling space air heating, Energy Convers. Manage. 201 (2019) 112151.

[46] S. Mat, A.A. Al-Abidi, K. Sopian, M.Y. Sulaiman, A.T. Mohammad, Enhance heat transfer for PCM melting in triplex tube with internal–external fins, Energy Convers. Manage. 74 (2013) 223–236.

[47] W.-B. Ye, D.-S. Zhu, N. Wang, Numerical simulation on phase-change thermal storage/release in a plate-fin unit, Appl. Therm. Eng. 31 (2011) 3871–3884.

[48] P.T. Sardari, D. Giddings, D. Grant, M. Gillott, G.S. Walker, Discharge of a composite metal foam/phase change material to air heat exchanger for a domestic thermal storage unit, Renew. Energy (2019).

[49] M.A. Hamdan, I. Al-Hinti, Analysis of heat transfer during the melting of a phase-change material, Appl. Therm. Eng. 24 (2004) 1935–1944.

[50] Z. Li, A. Shahsavar, A.A. Al-Rashed, P. Talebizadehsardari, Effect of porous medium and nanoparticles presences in a counter-current triple-tube composite porous/nano-PCM system, Appl. Therm. Eng. 167 (2020) 114777.

[51] A.A. Al-Abidi, S. Mat, K. Sopian, M.Y. Sulaiman, A.T. Mohammad, Internal and external fin heat transfer enhancement technique for latent heat thermal energy storage in triplex tube heat exchangers, Appl. Therm. Eng. 53 (2013) 147–156.

[52] Y. Xu, Q. Ren, Z.-J. Zheng, Y.-L. He, Evaluation and optimization of melting performance for a latent heat thermal energy storage unit partially filled with porous media, Appl. Energy 193 (2017) 84–95.